CANCER

Monocytic MDSCs exhibit superior immune suppression via adenosine and depletion of adenosine improves efficacy of immunotherapy

Omar S. Sarkar[1]†, Howard Donninger[2,3,4]†, Numan Al Rayyan[2,3,5], Lewis C. Chew[3], Bryce Stamp[3]‡, Xiang Zhang[6], Aaron Whitt[7], Chi Li[2,3,4,7], Melissa Hall[3], Robert A. Mitchell[1,8,9], Alfred Zippelius[10], John Eaton[3,9], Jason A. Chesney[2,8,9], Kavitha Yaddanapudi[1,8,9]*

Immune checkpoint inhibitor (ICI) therapy is effective against many cancers for a subset of patients; a large percentage of patients remain unresponsive to this therapy. One contributing factor to ICI resistance is accumulation of monocytic myeloid-derived suppressor cells (M-MDSCs), a subset of innate immune cells with potent immunosuppressive activity against T lymphocytes. Here, using lung, melanoma, and breast cancer mouse models, we show that CD73-expressing M-MDSCs in the tumor microenvironment (TME) exhibit superior T cell suppressor function. Tumor-derived PGE_2, a prostaglandin, directly induces CD73 expression in M-MDSCs via both Stat3 and CREB. The resulting CD73 overexpression induces elevated levels of adenosine, a nucleoside with T cell–suppressive activity, culminating in suppression of antitumor $CD8^+$ T cell activity. Depletion of adenosine in the TME by the repurposed drug PEGylated adenosine deaminase (PEG-ADA) increases $CD8^+$ T cell activity and enhances response to ICI therapy. Use of PEG-ADA can therefore be a therapeutic option to overcome resistance to ICIs in cancer patients.

INTRODUCTION

The development of immune checkpoint inhibitors [ICIs; e.g., anti–PD-1 (programmed cell death protein 1) antibody (Ab)] has revolutionized the therapy of several malignancies including melanoma, non–small cell lung cancer (NSCLC), and, to a lesser extent, triple-negative breast cancer (*1*, *2*). Despite the clinical success of anti–PD-1 in cancer treatment, therapeutic resistance continues to occur in large percentages of patients. One of the best predictors of clinical responses to anti–PD-1 Ab is the presence of increased tumor somatic mutations (*3*). Relative mutational burden dictates neoantigen load that, in turn, elicits antitumor responses in the primary targets of anti–PD-1, i.e., the $CD8^+$ T cells (*4*, *5*). However, even among patients with high tumor neo-antigens and intrinsic numbers of antigen (Ag)–specific $CD8^+$ T cells, up to 50% remain unresponsive to anti–PD-1 (*5*, *6*). These findings strongly suggest the presence of additional mechanisms of immune suppression that directly confer resistance to anti–PD-1 and support combinatorial treatment strategies to improve systemic disease control and patient survivability.

Several mechanisms have been proposed to account for the immune suppression in tumor-bearing hosts. One widely studied process involves cancer-induced aberrations in myelopoietic output, which lead to the generation and accumulation of different immunosuppressive myeloid cells in the tumor microenvironment (TME) of many solid tumors. These tumor-educated myeloid-derived suppressor cells (MDSCs) actively inhibit $CD8^+$ T cell tumor homing and activation (*7*, *8*). We and others have demonstrated that among the tumor-induced MDSC subsets, monocytic MDSCs (M-MDSCs) have the greatest suppressive activity on $CD8^+$ T cells (*9*, *10*). Given that M-MDSC levels are elevated in human cancers (*11*, *12*) and associate with decreased patient survival (*13*, *14*), intervention strategies that can reverse M-MDSC–suppressive activity will support immunotherapy and enhance the durability of clinical response. Now, such strategies are limited.

A further process that leads to immune suppression in tumors is mediated by the purine nucleoside adenosine. Adenosine suppresses immune activity of T cells both directly by inhibiting activation of antitumor effector responses and indirectly by inducing expansion of other immune suppressive cell subtypes within the TME (*15*, *16*). Metabolic changes occurring within a growing tumor favor the increased accumulation of extracellular adenosine (*15*). The generation of this purine nucleoside occurs through the degradation of adenosine triphosphate (ATP) by the combined actions of enzymes CD39 [ectonucleoside triphosphate diphosphohydrolase; ATP → adenosine monophosphate (AMP)] and CD73 (ecto-5′-nucleotidase; AMP → adenosine) (*17*). The biological rationale for this adenosine accumulation in healthy individuals is to limit tissue damage in areas of injury. Cell damage arising from an injury leads to the release of intracellular ATP which is then converted to the anti-inflammatory compound adenosine. The latter, sensed by adenosine A2A receptors (*18*, *19*) expressed on the immune cells, has the net effect of putting the brakes on inflammatory responses; however, in the case of cancer, the same activity suppresses immunity and facilitates tumor growth and metastasis. Identification of

[1]Department of Microbiology and Immunology, University of Louisville, Louisville, KY, USA. [2]Department of Medicine, University of Louisville, Louisville, KY, USA. [3]James Graham Brown Cancer Center, University of Louisville, Louisville, KY, USA. [4]Experimental Therapeutics Program, University of Louisville, Louisville, KY, USA. [5]Natural Agricultural Research Center, P.O. Box 639, Baq'a 19381, Jordan. [6]Department of Chemistry, University of Louisville, Louisville, KY, USA. [7]Department of Pharmacology and Toxicology, University of Louisville, Louisville, KY, USA. [8]Department of Surgery, Division of Immunotherapy, University of Louisville, Louisville, KY, USA. [9]Immuno-Oncology Group, Brown Cancer Center, University of Louisville, Louisville, KY, USA. [10]Center for Immunotherapy, Cancer Center Medical Oncology, University Hospital Basel, Switzerland.
*Corresponding author. Email: kavitha.yaddanapudi@louisville.edu
†These authors contributed equally to this work.
‡Present address: University of North Carolina, Chapel Hill, NC, USA.

therapeutics that can effectively eliminate adenosine holds promise for disengaging the adenosine-mediated immune suppression in tumors.

Here, we show that prostaglandin E_2 (PGE_2) released from tumor cells directly induces expression of CD73 in M-MDSCs via a previously undescribed PGE_2 → cyclic AMP (cAMP) → cAMP response element–binding protein (CREB)/signal transducer and activator of transcription (STAT3)–dependent pathway. We examine the phenotypic and functional behavior of CD73-expressing M-MDSCs in the TME in human lung cancer and in several types of murine cancers. We show that PGE_2-induced CD73 sustains the immunosuppressive activity of M-MDSCs in the TME. We further show that CD73-expressing M-MDSCs exhibit superior T cell suppressor function via an adenosine-mediated mechanism.

To evaluate whether therapeutically targeting the immunosuppressive intratumoral adenosine can improve the efficacy of anti–PD-1 therapy, we use an innovative agent, polyethylene glycol-conjugated (PEGylated)–adenosine deaminase (PEG-ADA) (*20*). PEG-ADA is U.S. Food and Drug Administration (FDA)–approved as an enzyme replacement therapy for children with severe combined immunodeficiency (SCID) (*20*). This enzyme converts adenosine to the inert, non-immune suppressive metabolite, inosine. Our data indicate that depletion of adenosine by PEG-ADA relieves adenosine-mediated T cell immune suppression and sensitizes tumors to anti–PD-1 therapy.

RESULTS

Immunosuppressive CD73-expressing monocytes accumulate in tumors of patients with advanced NSCLC

Previously, we had demonstrated that the frequencies of $CD14^+HLA\text{-}DR^{low/-}$ M-MDSCs are substantially elevated in patients with advanced-stage melanoma, and we established an in vitro model of human M-MDSC induction using healthy donor monocytes cocultured with the melanoma cell line, A375 (*9*). A comparative microarray analysis of cultured monocytes and A375-educated monocytes (A375-MDSCs) revealed that several immunosuppressive mediators including interleukin-6 (IL-6), Indoleamine 2,3-dioxygenase 1 (IDO), and NADPH Oxidase 4 (NOX4) are differentially expressed in A375-M-MDSCs (*9*). One gene product of particular interest that was up-regulated to high levels in A375-MDSCs is the ecto-5′-nucleotidases CD73 (fig. S1A). Given that CD73 is centrally involved in generating adenosine, a potent immunosuppressive molecule in the TME (*21*), we validated the high expression levels of *CD73* mRNA in A375-MDSC by quantitative polymerase chain reaction (PCR; fig. S1B). Intriguingly, we found that the expression of *CD39* mRNA, an ecto-nucleoside triphosphate diphosphohydrolase enzyme that converts ATP to AMP, is down-regulated in A375-MDSCs (fig. S1, A and C).

To determine whether soluble factors released from the tumor cells influence CD39/CD73 expression in M-MDSCs, we cocultured A375 melanoma and A549 lung carcinoma cells with $CD14^+$ monocytes from healthy donors using an in vitro Transwell experimental system; monocytes cultured in tumor cell–free media were used as the control. As shown in Fig. 1 (A to C), CD73 expression is significantly higher in lung cancer- and melanoma-educated $CD14^+HLA\text{-}DR^{low/neg}$ monocytes when compared to that in monocytes cultured in media alone. In monocytes exposed to tumor cell media, we observed significant increases in the percentage of CD73-bearing cells (Fig. 1, A and B) as well as the relative expression levels of CD73 [mean fluorescence intensity (MFI); Fig. 1C]. The expression levels of CD39, on the other hand, were very low in both the cultured and tumor-educated monocytes (fig. S1D). We found that these tumor-educated $CD73^+$ monocytes significantly inhibited the proliferation of autologous T cells in an in vitro T cell–suppressive assay (Fig. 1, D and E).

We extended these tumor cell line–based studies to human primary tumors. CD73 expression was significantly higher in metastatic lung tumor–infiltrating $CD14^+HLA\text{-}DR^+CD68^{neg}CD15^{neg}CD16^{neg}$ monocytes when compared to CD73 expression in circulating $CD14^+$ monocytes (Fig. 1, F and G). Next, we assessed the contribution of CD73 enzymatic activity to adenosine generation and immune suppression in the lung TME. Analysis using liquid chromatography–mass spectrometry (LC-MS) revealed higher levels of adenosine in lung tumor tissue than in adjacent normal tissue (Fig. 1H and Fig. S2A). To characterize the functional phenotype of CD73-expressing $CD14^+$ monocytes from human NSCLC samples, we sorted these cells and examined their suppressive activity. Tumor-infiltrating CD73-expressing $CD14^+$ cells inhibited the anti-CD3/anti-CD28–induced proliferation of autologous $CD3^+$ T cells (Fig. 1I). While we recognize that there are other immunosuppressive myeloid subsets in the TME, such as tumor-associated macrophages, due to limitations in patient sample availability, we were unable to profile other myeloid subsets in this study. We are currently collecting more NSCLC patient samples to evaluate CD73 expression on all myeloid subsets, and this will be a focus of a future study.

Tumor-derived PGE_2 induces CD73 expression on tumor-associated monocytes

To determine which soluble factors from the tumor cells are responsible for the observed up-regulation of CD73, we exposed the $CD14^+$ monocytes isolated from healthy donors to previously reported suppressive factors released from tumor cells—granulocyte-macrophage colony-stimulating factor (GM-CSF), PGE_2, IL-6, and IL-4 or a combination of these factors. GM-CSF alone or GM-CSF + IL-6 or GM-CSF + IL-4 combinations did not markedly alter the surface CD73 expression on monocytes (Fig. 2, A and B). However, the short-term exposure of the monocytes to the GM-CSF + PGE_2 combination resulted in significantly enhanced levels of CD73 expression than that exhibited in monocytes exposed to GM-CSF alone (Fig. 2, A and B).

The addition of GM-CSF + PGE_2 to human $CD14^+$ monocytes isolated from healthy donors for a 6-day period promoted the development of $CD14^+CD33^+HLA\text{-}DR^{low/neg}$ M-MDSC–like cells. A large proportion of these cells expressed CD73 (Fig. 2, C and D) and displayed significant inhibitory activity against tetanus toxoid–activated T lymphocytes (Fig. 2E). Addition of GM-CSF alone did not induce M-MDSC differentiation and CD73 expression (Fig. 2, C and D). In contrast, addition of GM-CSF + IL-4 combination to monocytes for 6 days induced differentiation of monocyte-derived dendritic cells (mo-DCs) which lack CD73 expression and, expectedly, were functionally immunostimulatory and induced a significant increase in tetanus toxoid–specific T cell proliferation (Fig. 2E).

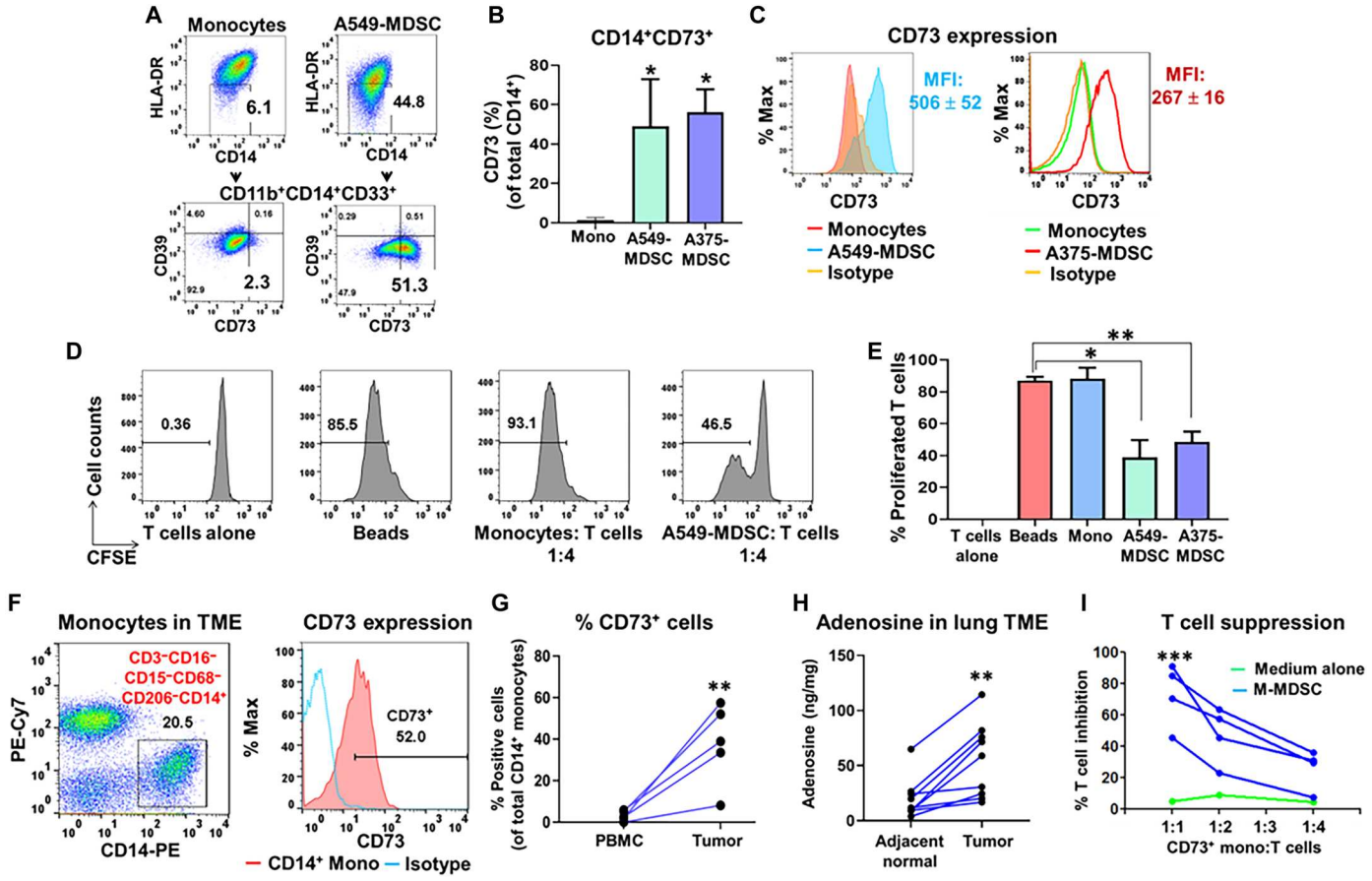

Fig. 1. Tumor-associated immunosuppressive myeloid cells express CD73. (**A** to **C**) $CD14^+$ monocytes from healthy donor peripheral blood mononuclear cells (PBMCs) were cocultured with tumor cells using a Transwell system. Representative dot plots (A), bar graph (B), and histograms (C) showing the expression of CD73 (proportions and MFI) in A549 and A375 tumor cell–induced human M-MDSCs. Data, mean ± SEM of three independent experiments with monocytes from three different donors. (**D** and **E**) Immune suppressive activity of A549- and A375-induced M-MDSCs. Autologous CFSE-labeled T cells were cultured in the presence of monocytes cultured for 64 hours in the absence of tumor cells (cultured mono) or with monocytes cocultured with A549 or A375 cells (A549-MDSC and A375-MDSC). T cells were activated with anti-CD3/anti-CD28 beads in the absence or presence of the indicated monocytes/MDSCs for 4 days. Representative histograms (D) and bar graph (E) show the percentage of proliferated CFSE-labeled T cells. Data, mean ± SEM of three independent experiments. (**F** and **G**) Human metastatic lung tumor–associated $CD14^+CD3^{neg}CD16^{neg}CD68^{neg}CD15^{neg}CD206^{neg}$ monocytes present in the tumors express higher levels of CD73 when compared to expression levels in the circulating monocytes. Data, mean ± SEM of $n = 5$ patients. Dot plot in (F) shows $CD14^+$ cells (*x* axis) versus CD3, CD16, CD68, CD15, and CD206 markers (*y* axis). PE-Cy7, Phycoerythrin-Cyanine 7. (**H**) Tumor and adjacent healthy tissues were resected from the same patients with NSCLC ($n = 9$ patients), and adenosine levels were quantified using LC-MS. (**I**) Immunosuppression mediated by human NSCLC-associated $CD73^+$ monocyte cells. $CD3^{neg}CD14^+CD73^+$ monocyte cells and autologous $CD3^+$ cells were sorted from fresh NSCLC cancer tissues and cocultured for 4 days in the presence of anti-CD3/anti-CD28 Ab. Representative line graph (I) showing the percentage of T cell inhibition. Data, mean ± SEM of cells from four different patients. *P* values: ***$P < 0.0005$; **$P < 0.005$; *$P < 0.05$.

$CD73^+$ M-MDSCs mediate superior T cell immunosuppression via adenosine

We further explored the immunosuppressive properties of CD73-expressing PGE_2–M-MDSCs by determining the immunosuppressive activity of purified $CD73^+$ and $CD73^{neg}$ PGE_2-induced M-MDSC subsets against anti-CD3/anti-CD28 Ab–activated autologous T cells. We found that the purified $CD73^+$ PGE_2–M-MDSC subfraction suppresses the proliferation of autologous T cells at levels comparable to that observed with tumor cell–induced M-MDSCs (Fig. 2F). The $CD73^{neg}$ PGE_2–M-MDSC subfraction had substantially lower T cell inhibitory activity confirming that the $CD73^+$ PGE_2–M-MDSC subset mirrors the recognized suppressive activity profile of tumor M-MDSCs (Fig. 2F). Reverse transcription PCR analysis showed a fourfold increase in *A2AR* gene expression in effector T cells within 48 hours of anti-CD3/anti-CD28–mediated T cell activation when compared to that in non-activated T cells (fig. S2B), corroborating the results presented in a previously published article (*17*). One likely scenario that rationalizes this is that $CD73^+$ PGE_2–M-MDSCs suppresses the T cell proliferation via the adenosine → A2AR pathway.

Next, we tested whether CD73 in PGE_2–M-MDSCs remains enzymatically active and can mediate adenosine production. $CD73^+$ and $CD73^{neg}$ PGE_2–M-MDSCs subfractions were cultured in the presence and absence of AMP, and adenosine levels in the supernatants were measured. $CD73^+$ PGE_2–M-MDSCs rapidly catalyzed the formation of adenosine from exogenously added AMP (Fig. 2G). The addition of ADA enzyme to $CD73^+$ M-MDSCs cultures markedly reduced the adenosine levels in the supernatants consistent

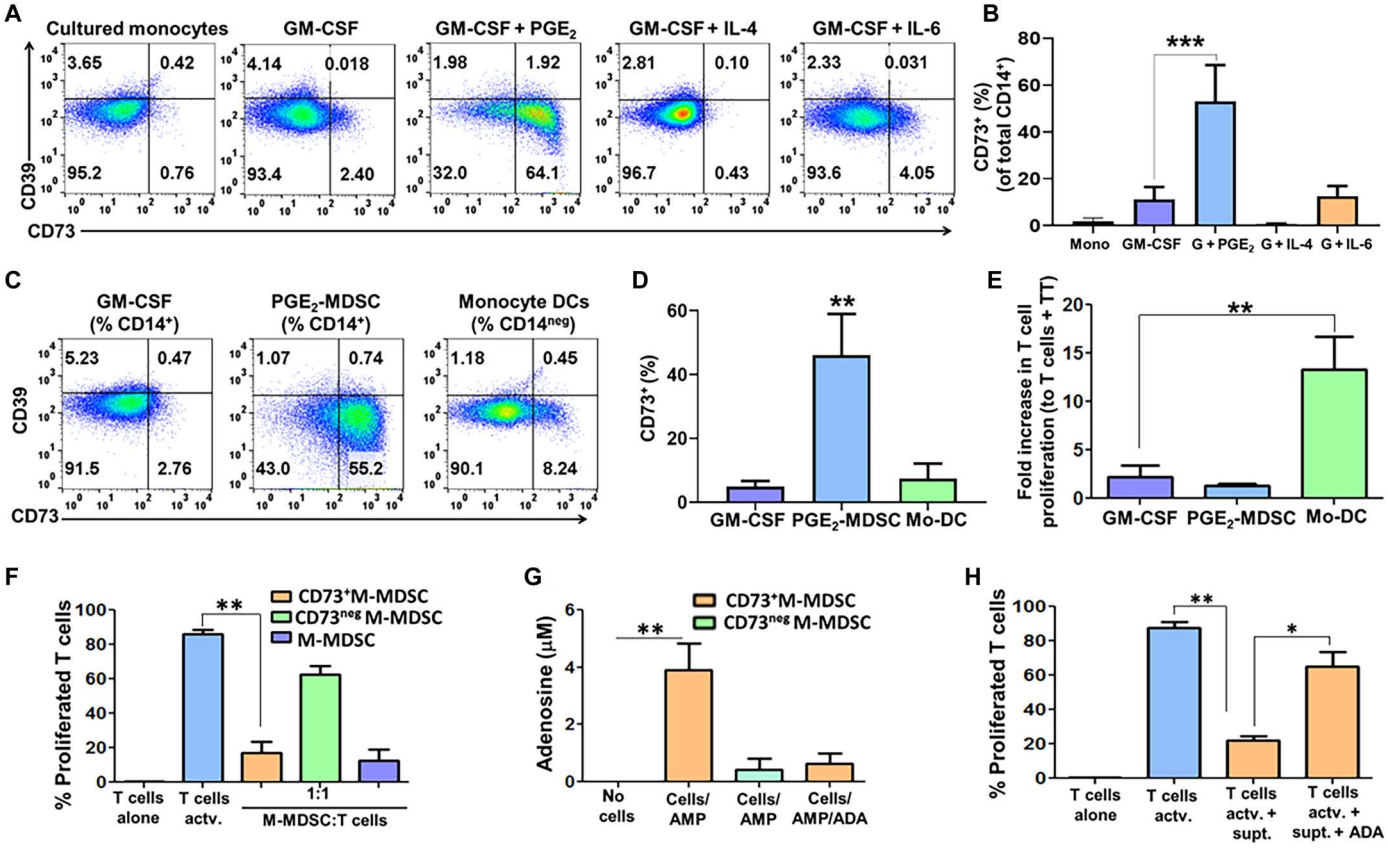

Fig. 2. PGE_2-induced $CD73^+$ M-MDSCs mediate immunosuppression via adenosine. (**A** and **B**) $CD14^+$ monocytes from healthy donors were either untreated (cultured monocytes) or treated for 48 hours with either GM-CSF (10 ng/ml), GM-CSF and PGE_2 (1 μM), IL-4 (10 ng/ml), or IL-6 (10 ng/ml), and CD73 expression was measured by flow cytometry. Representative dot plots (A) and bar graph (B) show the CD73 expression (%) in the treated cells. Data, mean ± SEM of three independent experiments with monocytes from three different donors. (**C** and **D**) $CD14^+$ monocytes from healthy donors were treated for 6 days with either GM-CSF, GM-CSF and PGE_2 (PGE_2-induced M-MDSCs), or GM-CSF and IL-4 [monocyte-derived dendritic cells (mo-DCs)]. Dot plots (C) and bar graph (D) show CD73 expression (%). Data, mean ± SEM of three independent experiments with monocytes from three different donors. (**E**) Indicated cells were added to autologous T cells in the presence of tetanus toxoid (TT; 1.0 μg/ml) for 5 days, and T cell proliferation was measured by incorporation of $^{[3H]}$thymidine. Data, mean ± SEM. (**F**) Immune suppressive activity (against anti-CD3/anti-CD28 bead–activated T cells) of $CD73^+$ or $CD73^{neg}$ PGE_2–M-MDSCs or tumor cell line–induced M-MDSCs. Data, mean ± SEM of three independent experiments. (**G**) Exogenous AMP (10 μM) or AMP and ADA (10 U/ml) were added to fresh medium with $CD73^+$ or $CD73^{neg}$ M-MDSCs for 6 to 8 hours. Extracellular adenosine was measured in the culture supernatants. Data, mean ± SEM of two independent experiments. (**H**) Untreated or ADA-treated culture supernatants from $CD73^+$ M-MDSCs cultured with AMP were added to T cells, and suppressive activity was measured by incorporation of $^{[3H]}$thymidine. Data, mean ± SEM of three independent experiments. *P* values: ***$P < 0.0005$; **$P < 0.005$; *$P < 0.05$.

with ADA's ability to degrade adenosine (Fig. 2G). In contrast, $CD73^{neg}$ M-MDSCs failed to generate extracellular adenosine from AMP in vitro (Fig. 2G). We then examined the T cell suppressive activity of adenosine in the $CD73^+$ M-MDSCs culture supernatants. Consistent with previous studies, addition of exogenous adenosine to human $CD3^+$ T cells suppressed their proliferation (fig. S2C). We observed that the adenosine in the $CD73^+$ M-MDSCs cell supernatants suppressed autologous T cell proliferation. Furthermore, addition of ADA enzyme abolished the T cell suppression mediated by $CD73^+$ M-MDSCs cell supernatants (Fig. 2H). These data confirm that PGE_2-induced $CD73^+$ M-MDSCs actively suppress T cell activity in an adenosine-dependent manner.

Both STAT3 and CREB are required for PGE_2-mediated regulation of CD73 expression in M-MDSCs

Next, we delineated the molecular mechanisms involved in PGE_2-induced CD73 expression. PGE_2 exerts its effects by relaying signals through the EP2 and EP4 cell surface receptors (*22*). Both receptors are expressed on PGE_2-MDSCs (fig. S3A). To determine which of these two receptors is primarily involved in PGE_2-mediated CD73 expression in M-MDSCs, $CD14^+$ monocytes were treated with either an EP2 or EP4 agonist in the presence of GM-CSF. The EP4 agonist only modestly increased CD73 levels, whereas the EP2 agonist-induced CD73 expression to levels comparable to that induced by PGE_2 (Fig. 3, A and B). Addition of IL-4 to the EP2 agonist–treated cells completely abolished CD73 expression (Fig. 3, A and B), suggesting that the EP2 receptor is preferentially responsible for PGE_2-mediated CD73 induction in MDSCs.

One of the effectors of EP2 → PGE_2 signaling is nuclear factor κB (NF-κB) (*23*). PGE_2 resulted in a marked activation of NF-κB

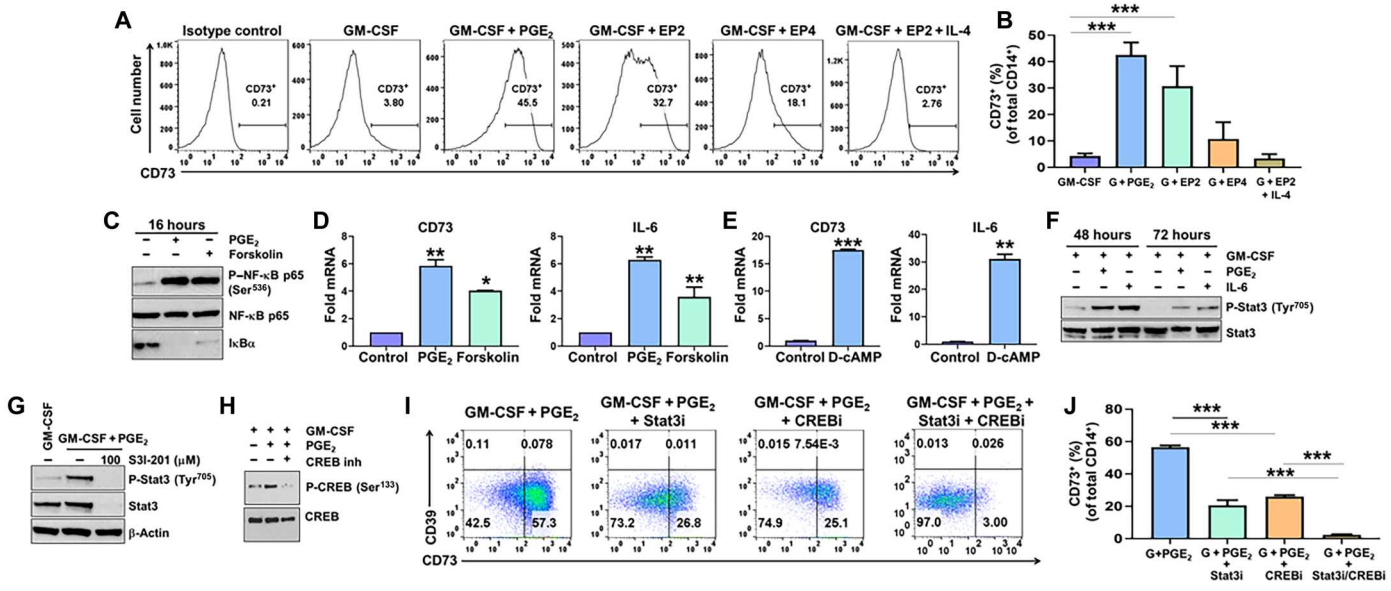

Fig. 3. Tumor-derived PGE_2 regulates CD73 expression in M-MDSCs via both a CREB and STAT3-dependent mechanism. (**A** and **B**) $CD14^+$ monocytes from healthy donors were treated with either GM-CSF (10 ng/ml), GM-CSF + PGE_2 (1 μM), GM-CSF + EP2 receptor agonist (butaprost; 10 μM), GM-CSF + EP4 receptor agonist (CAY10598; 10 nM), or GM-CSF + IL-4 (10 ng/ml) + EP2 receptor agonist for 6 days. CD73 expression was measured by flow cytometry. Data, mean ± SEM of three independent experiments. (**C**) $CD14^+$ monocytes are treated with either vehicle (Control), PGE_2 (1 μM), or Forskolin (10 μM) for 16 hours, and NF-κB activation was measured by Western blot. (**D**) Bar graphs showing the *CD73* and *IL-6* mRNA expression in $CD14^+$ monocytes treated as in (C). Data, mean ± SEM. (**E**) Bar graphs showing the *CD73* and *IL-6* mRNA expression in $CD14^+$ monocytes treated with either vehicle (Control) or D-cAMP (100 μM) for 16 hours. Data, mean ± SEM. (**F**) $CD14^+$ monocytes were treated with either GM-CSF (10 ng/ml), GM-CSF + PGE_2 (1 μM), or GM-CSF + IL-6 (10 ng/ml) for 48 and 72 hours, and activation of Stat3 was assessed by Western blot. (**G**) $CD14^+$ monocytes were treated with either GM-CSF alone, GM-CSF + PGE_2/vehicle, or GM-CSF + PGE_2/Stat3 inhibitor (S3I-201; 100 μM) for 48 hours, and Stat3 activation was assessed by Western blot. (**H**) $CD14^+$ monocytes were treated with either GM-CSF alone, GM-CSF + PGE_2/vehicle, or GM-CSF + PGE_2/CREB inhibitor (666-15; 2 μM) for 48 hours, and CREB activation was assessed by Western blot. (**I** and **J**) $CD14^+$ monocytes were treated with either Stat3, CREB, or Stat3/CREB inhibitors as in (G) and (H), and CD39/CD73 expression was measured. Data, mean ± SEM of three independent experiments. *P* values: ***$P < 0.0005$; **$P < 0.005$; *$P < 0.05$.

signaling as evidenced by an increase in phospho–NF-κB and degradation of IκBα (an inhibitor of NF-κB; Fig. 3C) and, as expected, resulted in an increase in *CD73* expression (Fig. 3D) along with a sharp increase in *IL-6* expression, a downstream target of NF-κB (Fig. 3D) (*24*, *25*). Addition of Forskolin, an activator of adenylate cyclase (*26*, *27*), to the monocytes, mimicked the effects of exogenous PGE_2 on NF-κB, *CD73*, and *IL-6* (Fig. 3, C and D). Similarly, addition of dibutyryl-cAMP (D-cAMP), a synthetic analog of cAMP (*28*), induced *CD73* and *IL-6* to similar levels as seen with PGE_2 (Fig. 3E). Together, these data suggest that PGE_2 induces CD73 expression by modulating the levels of cAMP and subsequent activation of NF-κB. PGE_2 also increased *IL-10* expression which was also mimicked by Forskolin and D-cAMP (fig. S3, B and C). However, while an anti–IL-10 Ab was effective at reducing PGE_2-induced IL-10 expression, it had no effect on PGE_2-induced CD73 expression (fig. S3, D and E), suggesting that IL-10 is not involved in PGE_2-mediated CD73 expression in M-MDSCs. While addition of IL-6 alone is not sufficient to induce CD73 expression in MDSCs (Fig. 2, A and B), it may still be playing a role in PGE_2-mediated CD73 induction as the IL-6 receptor is expressed on both PGE_2- and IL-6–stimulated monocytes (fig. S3F). One of the key downstream mediators of IL-6 signaling is Stat3 (*29*). Addition of PGE_2 resulted in significant activation of Stat3 which was comparable to that observed by addition of IL-6 alone (Fig. 3F). Inhibition of Stat3 with a Stat3 inhibitor resulted in an approximately 50% reduction in CD73 expression (Fig. 3, G, I, and J), suggesting that PGE_2-induced CD73 expression is, in part, mediated by Stat3 activation. Since inhibition of Stat3 only partially blocked PGE_2-induced CD73 expression, this suggested the involvement of an additional signaling pathway(s). cAMP also activates protein kinase A, which in turn activates CREB, a transcription factor (*30*). Addition of GM-CSF and PGE_2 to monocytes resulted in activation of CREB (Fig. 3H). Inhibition of CREB with a CREB inhibitor again reduced PGE_2-induced CD73 by only approximately 50% (Fig. 3, H to J). Addition of both the Stat3 inhibitor and the CREB inhibitor resulted in a complete loss of PGE_2-induced CD73 expression (Fig. 3, I and J). These results suggest that both Stat3 and CREB are required for PGE_2-induced CD73 expression.

Genetic deletion of PGE_2 reduces levels of $CD73^+$ M-MDSCs in the TME

We next used murine bone marrow (BM)–derived MDSCs to test our hypothesis that tumor-derived PGE_2 regulates T cell suppressive activity of M-MDSCs in a CD73-dependent manner. We cultured whole BM cells for 5 days with GM-CSF alone, GM-CSF + PGE_2, or GM-CSF + IL-4 and monitored the induction of CD73 in these cells. Short-term BM cultures in the presence of GM-CSF alone or GM-CSF + PGE_2 combination resulted in the generation of cells with $CD11b^{hi}Gr\text{-}1^{int}$ M-MDSC subset as shown previously (*10*, *31*) (Fig. 4A).

Our data now show that both the proportions of $CD73^+$ and relative expression (MFI) of CD73 were negligible in freshly isolated

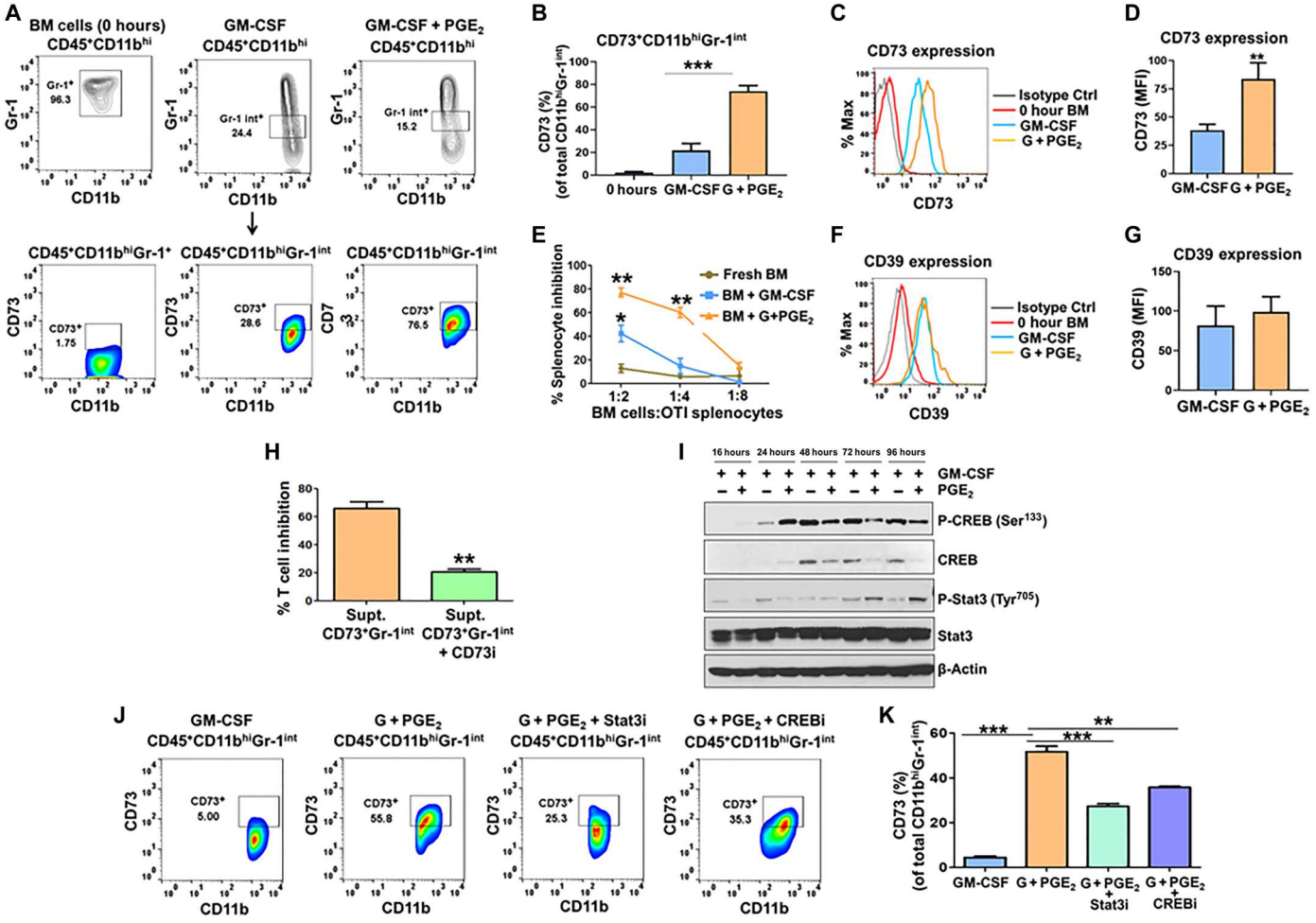

Fig. 4. PGE_2-induced murine BM-derived $CD73^+$ M-MDSCs exhibit heightened immunosuppressive activity. (**A** and **B**) Murine BM cells from C57BL/6 mice were cultured with GM-CSF (20 ng/ml) or GM-CSF/PGE_2 (2.6 μM) for 5 days. Accumulation of $CD45^+CD11b^{hi}Gr\text{-}1^{int}$ M-MDSC cells and proportions of $CD73^+$ cells in $CD45^+CD11b^{hi}Gr\text{-}1^{int}$ M-MDSC population are shown in representative contour and dot plots (A) and bar graph (B), respectively. Data, mean ± SEM of three independent experiments. (**C**, **D**, **F**, and **G**) Histograms and bar graphs showing expression of CD73 (C) and (D) and CD39 (F) and (G) in total $CD11b^{hi}Gr\text{-}1^{int}$ BM cells. (**E**) Fresh BM cells or BM cells treated as in (A) were added to splenocytes from OT-I transgenic mice at 1:2, 1:4, and 1:8 ratio in the presence of OVA (250 μg/ml) per well for 4 days. T cell proliferation was measured by $^{[3H]}$thymidine incorporation. Data, mean ± SEM of three independent experiments. (**H**) $CD73^+$ BM-MDSCs were purified and cultured with AMP in the presence or absence of CD73 inhibitor AMP-CP (10 μM), and supernatants were added to T cells in the presence of anti-CD3 and anti-CD28 antibodies. T cell proliferation was measured by $^{[3H]}$thymidine incorporation. Data, mean ± SEM of three independent experiments. (**I**) BM cells were cultured with either GM-CSF alone or GM-CSF + PGE_2 for 16, 24, 48, 72, and 96 hours, and Stat3 and CREB activation was assessed by Western blot. β-Actin was used as a loading control. (**J** and **K**) BM cells are treated with either GM-CSF alone, GM-CSF + PGE_2/vehicle, or GM-CSF + PGE_2/Stat3 inhibitor (S3I-201; 100 μM) or GM-CSF + PGE_2/CREB inhibitor (666-15; 1 μM) for 72 hours and analyzed by flow cytometry. Data, mean ± SEM of two independent experiments. *P* values: ***$P < 0.0005$; **$P < 0.005$; *$P < 0.05$.

$CD11b^{hi}Gr\text{-}1^+$ BM cells (Fig. 4, A, B, and D). These cells did not have T cell inhibitory activity when added at different concentrations to ovalbumin (OVA)–stimulated splenocytes obtained from OT-1 mice (Fig. 4E). Addition of GM-CSF to BM cells induced a moderate increase in the proportions and expression of CD73 in $CD11b^{hi}Gr\text{-}1^{int}$ cells and, accordingly, displayed moderate ability to suppress the OVA Ag–specific T cell proliferation (Fig. 4, A to E). The addition of the cytokine combination GM-CSF + IL-4 to BM cells for 5 days resulted in the enrichment of $CD11b^+Gr\text{-}1^{neg}CD11c^+$ dendritic cells that lacked CD73 expression and were unable to suppress OVA Ag–stimulated T cells (fig. S4, A and B). In alignment with our ex vivo human data, treatment of BM cells with GM-CSF + PGE_2 combination induced a significant increase in the proportions of CD73-expressing BM-MDSCs. These PGE_2-induced BM-MDSCs have superior T cell inhibitory activity (Fig. 4, A to E). We observed that in contrast to human monocytes, BM cells treated with GM-CSF showed increased expression of CD39 on their cell surface. However, these expression levels were not further altered with the addition of PGE_2 (Fig. 4, F and G). To directly determine whether CD73 is functionally active, AMP was added to PGE_2–BM–MDSCs exogenously in the presence or absence of the CD73 inhibitor AMP-CP, and the culture supernatants were collected. The supernatants from untreated $CD73^+$–BM–MDSCs suppressed the anti-CD3/anti-CD28–induced T cell proliferation, and the CD73 inhibitor rescued the T cell proliferation (Fig. 4H).

To confirm the involvement of both CREB and Stat3 in PGE_2-induced CD73 expression in the human system (Fig. 3), we performed a similar experiment using murine BM cells treated with either GM-CSF alone or GM-CSF + PGE_2 and found that both CREB and Stat3 were activated when the cells were treated with PGE_2, with CREB being activated 24 hours after PGE_2 addition and Stat3 being activated 72 hours after PGE_2 treatment with maximal activation at 96 hours (Fig. 4I). We found that while the Stat3 protein was continuously expressed over all time points tested, CREB appeared to show a delayed expression pattern, with the protein only appearing 24 hours after addition of PGE_2. In addition, while there was clear activation of CREB at the early time points of MDSC differentiation, CREB activation decreased at later time points (Fig. 4I). This could be due to differences in the human and mouse in vitro PGE_2-induced MDSC differentiation systems. The requirement for both Stat3 and CREB for maximal expression of CD73 was confirmed by flow cytometry using Stat3 and CREB inhibitors individually, which only partially reduced CD73 expression in the PGE_2-treated BM cells (Fig. 4, J and K).

To validate our ex vivo data in a localized TME in vivo in mice, we initially measured PGE_2 levels in vitro in a panel of three syngeneic immunocompetent mouse tumor models—B16 melanoma, Lewis lung carcinoma (LLC), and 4T1 breast carcinoma. Using enzyme-linked immunosorbent assay (ELISA), we measured the baseline levels of PGE_2 produced by the tumor cell lines. The data showed that B16-F10 melanoma and LLC cells produce low levels of PGE_2, while 4T1 cells produce high levels of PGE_2 into the culture supernatants (Fig. 5A).

To confirm our hypothesis that tumor-derived PGE_2 influences CD73 expression in myeloid cells, we stably knocked down *PTGES* (prostaglandin E synthase, an enzyme critical for the synthesis of PGE_2) in 4T1 cells (4T1-*shPTGES*) using short hairpin RNA technology, thereby blocking PGE_2 production in the tumor cells (Fig. 5A). We then established subcutaneous B16-F10, LLC, 4T1-shScr, and 4T1-*shPTGES* tumors in syngeneic mice. Tumors were harvested 18 to 21 days posttumor cell injection, and the CD73 expression was profiled in MDSCs present in the tumor digests. Our data show that the frequencies of CD73-expressing $CD11b^{hi}GR\text{-}1^{int}$ M-MDSCs are significantly higher in tumors with higher PGE_2 levels (Fig. 5, B to D); we observed a strong correlation between PGE_2 levels and $CD73^+$ M-MDSC frequencies in these tumor models (Fig. 5E). We also compared the CD73 expression levels between $CD11b^{hi}Gr\text{-}1^{int}$ M-MDSCs and $CD11b^{hi}Gr\text{-}1^{hi}$ granulocytic MDSCs (G-MDSCs) (*10*) subsets in 4T1 tumors. The G-MDSC subpopulation expressed low levels of CD73 (Fig. 5F), and hence, no correlation was observed between PGE_2 levels and CD73-expressing G-MDSCs present in the tumors. These data indicated that the induction of CD73 expression on M-MDSCs but not on G-MDSC was reliant on PGE_2 expression from within the tumors.

Deletion of CD73 mitigates adenosine-dependent immunosuppression by M-MDSCs in tumors

To evaluate the in vivo functional contributions of the PGE_2 synthesis pathway to the expansion of immunosuppressive $CD73^+$ M-MDSCs in a physiologically relevant environment, we established an orthotopic KP1.9 lung adenocarcinoma mouse model. KP1.9 cells are originally isolated from *LSL-Kras*^{G12D}*: p53*$^{fl/fl}$ (KP) transgenic mouse model of NSCLC (*32*). Our data from the orthotopic KP1.9 mouse model show that tumor development in the mouse lungs initiates around day 24 posttumor cell injection and progressively intensifies until days 40 to 42; (Fig. 6, A and B).

PGE_2 levels were high in these tumors, with an average of 189 ± 48 ng of PGE_2 present per gram of tumor tissue (Fig. 6C). We also found that a significant percentage of M-MDSCs expressed CD73 in the KP tumor–bearing lungs when compared to a similar population of monocytes present in lungs obtained from naïve mice (Fig. 6, D and E). CD73–M-MDSC functionality in KP lung tumors was determined using the OT-I T cell receptor (TCR) transgenic mice and OVA Ag presentation. Our data indicate that CD73-expressing KP lung tumor–derived M-MDSCs significantly suppressed OVA Ag–specific $CD8^+$ T cell proliferation, while monocytes derived from naïve lungs failed to exhibit any T cell–suppressive activity (Fig. 6F). In addition, adenosine-containing culture supernatants from the $CD73^+$ M-MDSCs from KP mice mediated potent suppression of anti-CD3/anti-CD28–induced T cell proliferation (Fig. 6G). We validated our observations in CD73-deficient mice ($Nt5e^{-/-}$). Orthotopic KP lung tumors were established in wild-type and $Nt5e^{-/-}$ mice (Fig. 6H). We found that M-MDSCs from $Nt5e^{-/-}$ were less immunosuppressive than wild-type M-MDSC cells (Fig. 6, I and J).

Next, we treated KP1.9 tumor–bearing mice with wild-type and $Nt5e^{-/-}$ BM-derived M-MDSCs (Fig. 6K) or M-MDSCs obtained from lung tumors (Fig. 6L). We found that tumor volumes were larger in mice that received wild-type M-MDSC cells than in those administered with $Nt5e^{-/-}$ M-MDSCs (Fig. 6, K and L), which suggested that $Nt5e^{-/-}$ M-MDSC cells were less suppressive than wild-type $Nt5e^{+/+}$ M-MDSCs in vivo in the KP1.9 tumor model.

Adenosine deaminase depletes intratumoral adenosine, enhancing tumor response to immunotherapy

We propose a unique and effective immunotherapeutic strategy involving the administration of adenosine deaminase (ADA)—an enzyme that specifically and irreversibly converts T cell–suppressive adenosine into the non-immunosuppressive nucleoside inosine. The PEGylated version of ADA (PEG-ADA) is an FDA-approved biologic that is currently used as an enzyme replacement therapy for ADA deficiency in pediatric SCID patients (*20*). PEG-ADA is a conjugate of numerous strands of monomethoxy PEG (5000 Da) covalently attached to the enzyme ADA. The enzyme ADA is involved in purine metabolism; it breaks down adenosine from food and is required for the turnover of nucleic acids in tissues (*33*, *34*). We have begun to test the idea that enzymatic conversion of adenosine to inosine in tumors might facilitate their destruction by $CD8^+$ T cells. To evaluate whether enzymatic conversion of adenosine to inosine is a viable immunotherapeutic approach, we initially assessed the potential efficacy of PEG-ADA to induce immune cell–mediated rejection of lung tumors using an implantable KP1.9 lung adenocarcinoma mouse model (*32*). C57BL/6 mice were injected subcutaneously with KP1.9 cells, and PEG-ADA or phosphate-buffered saline (PBS; vehicle control) was injected intraperitoneally on day 0 and then every 2 days for 28 days. As shown in Fig. 7A, KP1.9 tumors in PEG-ADA–treated mice were significantly smaller and grew at a much slower rate than those in control mice.

Because extracellular adenosine promotes evasion from antitumor T cell responses, we set out to determine whether PEG-ADA–mediated catabolism of intratumoral adenosine might alter protumorigenic T cell responses in tumor-bearing mice. We

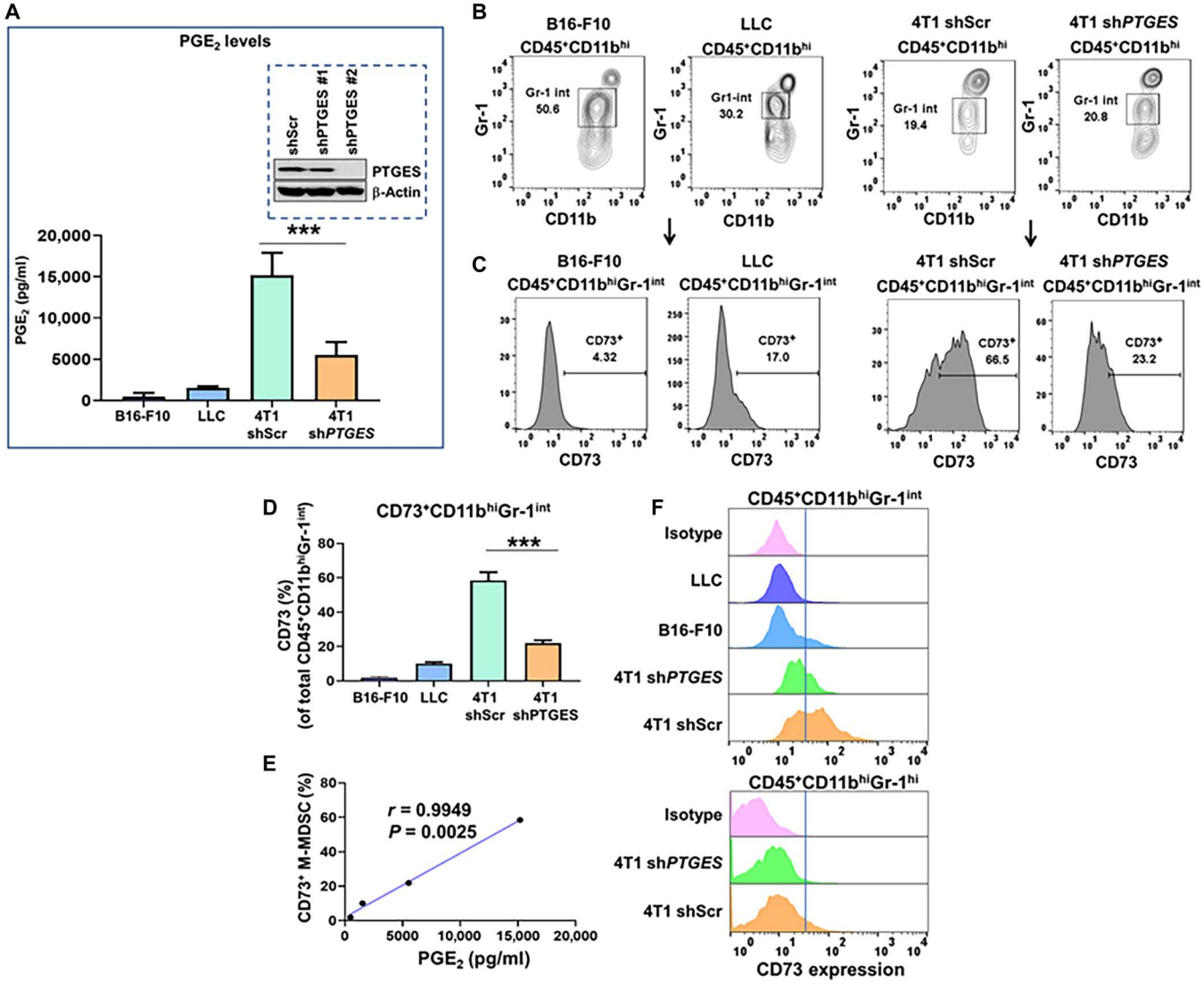

Fig. 5. Genetic depletion of tumor-derived PGE_2 reduces CD73 expression on M-MDSCs in the TME. (**A**) Bar graphs showing PGE_2 levels in culture supernatants of murine B16-F10 melanoma cells, LLC lung cancer cells, and 4T1 breast cancer cells with either *PTGES* knockdown or scrambled control (4T1*shPTGES*, 4T1shScr, inset) as measured by ELISA ($n = 2$ independent ELISA expt.). Data, mean ± SEM. (**B** to **F**) Syngeneic tumors implanted subcutaneously into BALB/c mice (4T1*shPTGES* and 4T1shScr cells) and C57BL/6 mice (B16-F10 and LLC cells) ($n = 5$ mice per tumor type). Tumors were isolated (800 to 1000 mm^3), digested, and stained for CD45, CD11b, Gr-1, and CD73 expression. Contour plots showing the proportions of $CD45^+CD11b^{hi}Gr\text{-}1^{int}$ M-MDSCs (B) and histograms (C) and bar graph (D) showing % $CD73^+$ cells within the $CD45^+CD11b^{hi}Gr\text{-}1^{int}$ M-MDSC population in the implanted tumors. Data, mean ± SEM. (E) Correlation between intratumoral % $CD73^+$ M-MDSCs versus PGE_2 levels produced by the corresponding tumor cells. $P = 0.0025$, $r^2 = 0.9949$. (F) Histograms showing CD73 expression in the $CD45^+CD11b^{hi}Gr\text{-}1^{int}$ M-MDSC and $CD45^+CD11b^{hi}Gr\text{-}1^{hi}$ G-MDSC population in the implanted tumors. *P* values: ***$P < 0.0005$.

assessed the quantity and quality of antitumor immune cell responses generated within the KP1.9 tumors in the PEG-ADA–treated and vehicle-treated (control) mice. For analysis of tumor-infiltrating immune cells, tumors from drug-treated and control mice were excised at the end of therapy and analyzed for expression of surface and functional markers of T cells by flow cytometry. Our data indicate that significantly higher frequencies of interferon-γ (IFN-γ)– and tumor necrosis factor–α (TNF-α)–producing $CD8^+$ T cells were obtained from PEG-ADA–treated tumors than that observed in the vehicle-treated tumors (Fig. 7B), while intratumoral adenosine levels were reduced (Fig. 7C). Our data indicate that the antitumor efficacy of PEG-ADA is associated with significantly lower levels of tumor growth–promoting intratumoral T regulatory cells and macrophages and higher levels of antitumor immunity–inducing neutrophils (Fig. 7D). In addition, the frequencies of dendritic cells were modestly increased, while the frequencies of M-MDSCs were somewhat lower in tumors from PEG-ADA–treated mice (Fig. 7D). These results suggest that PEG-ADA treatment reduces intratumoral adenosine levels and, consequently, generates antitumor T cell responses. This illustrates the important point that PEG-ADA may also be useful to treat tumors with high baseline levels of PGE_2/adenosine. PEG-ADA functionally synergizes with anti–PD-1 Ab to reduce KP1.9 cells' resistance to anti–PD-1 monotherapy resulting in significantly reduced subcutaneous tumor

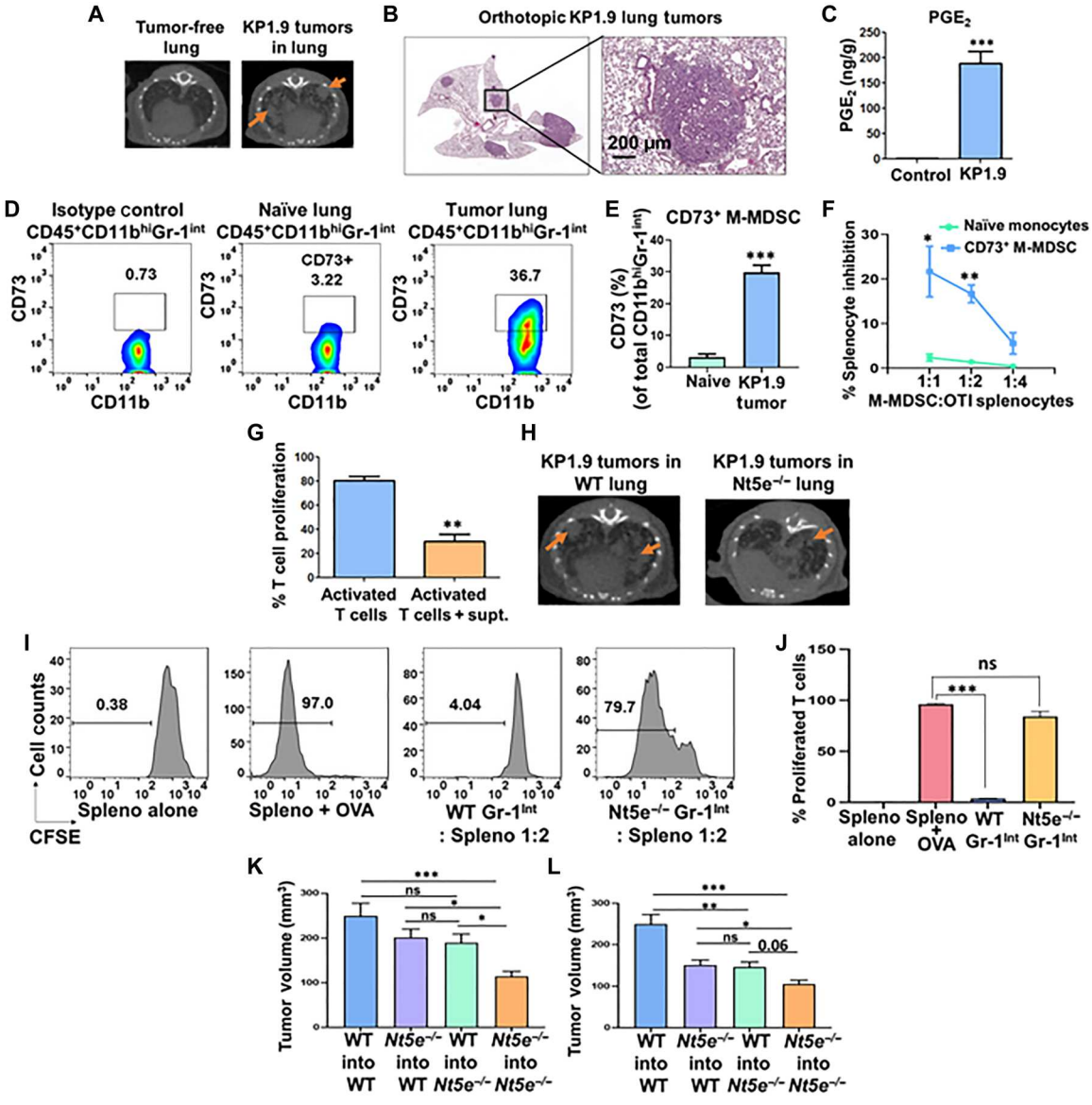

Fig. 6. Genetic deletion of CD73 reduces the adenosine-dependent suppressive activity of M-MDSCs in the TME. (**A** to **G**) C57BL/6 mice ($n = 20$) were injected with KP1.9 cells intravenously. (A) Representative micro-CT images of lungs at day 40. Red arrows, individual tumor. (B) Hematoxylin and eosin–stained section of tumor-bearing mouse lung. Magnification: ×1 and ×8. (C) Bar graph showing PGE_2 levels in the lung tissue measured using mass spectrometry ($n = 4$). Data, mean ± SEM. Dot plots (D) and bar graph (E) show % $CD73^+$ cells within the $CD45^+CD11b^{hi}Gr\text{-}1^{int}$ population in naïve and tumor-bearing mouse lungs. (F) $CD73^+$ $CD45^+CD11b^{hi}$-$Gr\text{-}1^{int}$ cells from lung tissue from tumor-bearing and naïve mice ($n = 6$ per group) were cocultured with OT-I splenocytes and OVA (250 μg/ml) for 4 days. T cell proliferation was measured using $^{[3H]}$-thymidine incorporation. Data, mean ± SEM. (G) Culture supernatants from $CD73^+$ M-MDSCs/AMP cultures were added to T cells, and proliferation was measured as above. Data, mean ± SEM of two independent experiments. (**H**) Representative micro-CT images of lungs from wild-type (WT) and $Nt5e^{-/-}$ KP1.9 mice, imaged at day 40. Red arrows, individual tumors. (**I** and **J**) M-MDSCs from wild-type and $Nt5e^{-/-}$ KP1.9 tumor–bearing mice were cocultured with CFSE-labeled splenocytes from OT1 mice and OVA (250 μg/ml) for 4 days, and $CD8^+$ T proliferation was measured by flow cytometry. Data, mean ± SEM of two independent experiments ($n = 6$). (**K** and **L**) Wild-type or $Nt5e^{-/-}$ mice were injected subcutaneously with KP1.9 cells (1.5×10^5) mixed with either wild-type or $Nt5e^{-/-}$ BM-derived M-MDSCs or lung tumor–derived M-MDSCs (2×10^5) ($n = 5$ to 7 per group). Bar chart represents tumor volumes. Data, mean ± SEM. *P* values: ***$P < 0.0005$; **$P < 0.005$; *$P < 0.05$; ns, not significant.

burden (Fig. 7E) and increased survival (Fig. 7F), suggesting that PEG-ADA therapy enhances anti–PD-1 Ab therapeutic efficacy. As a further test of the effects of PEG-ADA on the growth of tumors akin to a therapeutic setting, we administered intraperitoneal injections of PEG-ADA starting at day 7 posttumor implantation followed by injections every other day. Our data indicate that, in this setting, PEG-ADA functionally synergizes with anti–PD-1 Ab resulting in significantly reduced subcutaneous tumor burden (Fig. 7G). We also assessed the potential efficacy of PEG-ADA to induce immune rejection of tumors using an orthotopic 4T1 mammary carcinoma mouse model. As shown in Fig. 7H, 4T1

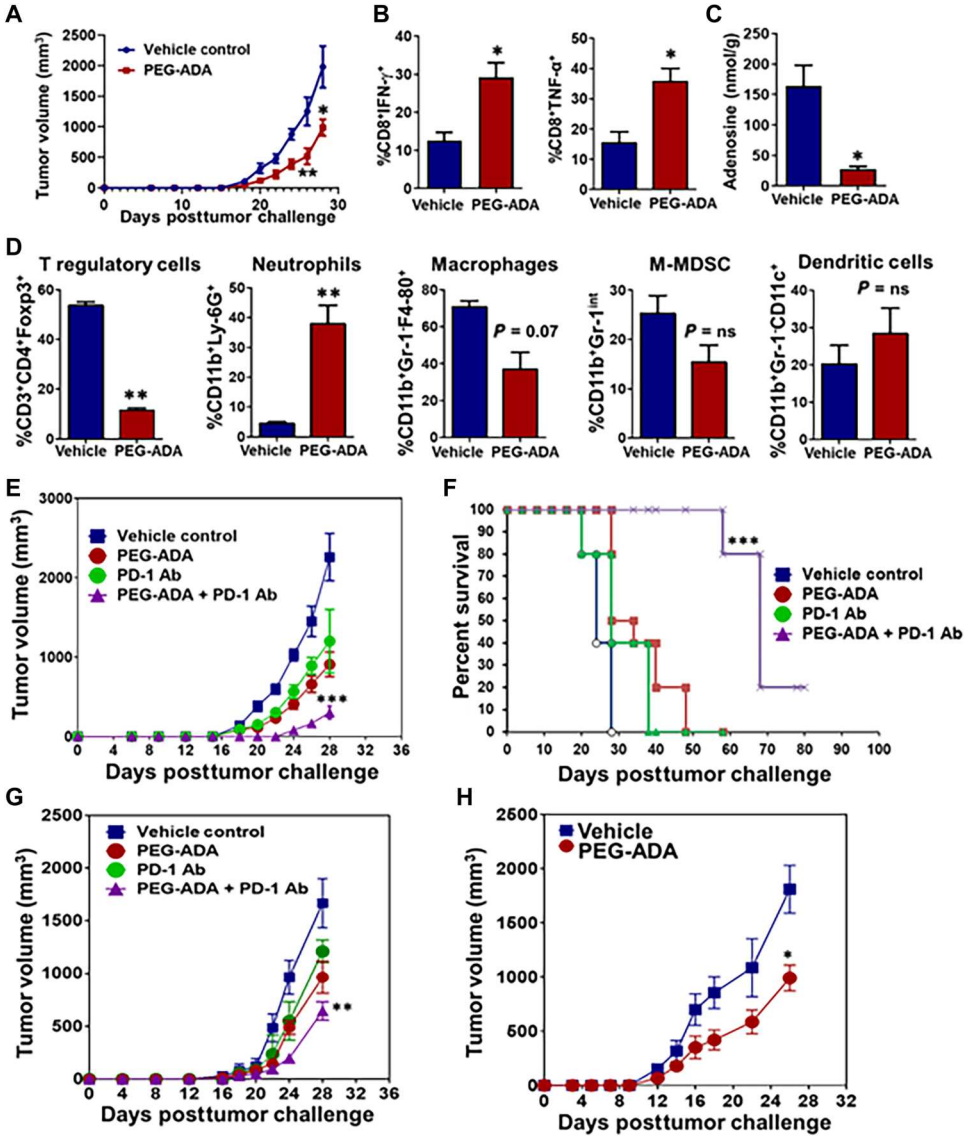

Fig. 7. PEG-ADA depletes intratumoral adenosine and enhances tumor response to anti–PD-1 immunotherapy. (**A**) C57BL/6 mice were injected subcutaneously with KP1.9 lung adenocarcinoma cells (2×10^5). PEG-ADA (2 U per mouse) or PBS (vehicle) was injected on day 0 and then every other day via intraperitoneal route, and tumor volume was measured. Data, mean ± SD of $n = 20$ mice per group; P values: $^*P \le 0.05$; $^{**}P \le 0.005$; relative to control group. (**B**) Bar graphs showing percentages of $CD45^+CD3^+CD8^+IFN\text{-}\gamma^+$ and $CD45^+CD3^+CD8^+TNF\text{-}\alpha^+$ cells in tumors derived from vehicle- and PEG-ADA–treated mice ($n = 5$ per group). Results are expressed as percentages of total $CD45^+$ cells. Data, mean ± SEM ($n = 6$ mice per group). P values: $^*P \le 0.05$. (**C** and **D**) Bar graphs showing adenosine levels and tumor-infiltrating immune cells in KP1.9 tumors derived from vehicle- and PEG-ADA–treated mice. Data, mean ± SEM of $n = 3$ to 5 mice per group, P values: $^*P \le 0.05$; $^{**}P \le 0.005$. (**E** to **G**) C57BL/6 mice were injected with KP1.9 cells at 2×10^5 cells per mouse subcutaneously. Starting either on day 0 (E) and (F) or day 7 (G) posttumor implantation, mice received the following treatments via the intraperitoneal route: (1) vehicle control (PBS); (ii) anti–PD-1 alone (250 μg per mouse); (iii) PEG-ADA alone (2 U per mouse); and (iv) anti–PD-1 plus PEG-ADA. Tumor sizes were plotted as tumor volume/time (E) and (G). Data, mean ± SD of $n = 8$ mice per group; P values: $^{***}P < 0.0005$; $^{**}P \le 0.005$; relative to vehicle-treated group. (F) Kaplan-Meier survival curves. $^{***}P < 0.0005$; log-rank test. (**H**) Female Balb/c mice were injected with 4T1 mammary carcinoma cells (2.0×10^5) in the mammary fat pads to establish orthotopic tumors, mice were treated as in (A), and tumor volume was measured. Data, mean ± SD of $n = 10$ mice per group, P values: $^*P \le 0.05$; relative to control group.

tumors in PEG-ADA–treated mice were modestly but significantly smaller.

DISCUSSION

MDSC-mediated suppressive activity is hypothesized to be one of the more prevalent mechanisms that provide an obstacle to immune-based therapeutic intervention (*35*). MDSCs inhibit antitumor T cell activity, thereby promoting an immunosuppressive milieu within the TME (*12*, *36*). As expected, advanced cancer patients with higher levels of MDSCs before treatment display a lower response to anti–PD-1 therapy (*13*, *37*, *38*). We show here that a prominent mechanism for the creation of the immunosuppressive environment within the tumors involves the $PGE_2 \rightarrow CD73^+$ M-

MDSC → Adenosine pathway. Our data show that the tumor cell–derived PGE_2 regulates CD73 expression in M-MDSCs and that CD73 expression sustains the M-MDSC–suppressive function leading to adenosine-dependent inhibition of $CD8^+$ T cell activation.

Despite the prominence of adenosine in driving cancer progression, no efficacious therapeutic strategy that specifically targets adenosine in solid tumors is currently available. Here, we illustrate an innovative treatment strategy that repurposes a clinically tested drug that achieves regression of most of the tumors in an anti–PD-1 treatment-resistant, clinically relevant lung cancer mouse model; we demonstrate that enzymatic depletion of intratumoral adenosine with PEG-ADA improves the therapeutic efficacy of anti–PD-1 Ab (Fig. 8).

Apoptotic T and natural killer regulatory cells in the TME have been shown to express CD73 and inhibit T cell responses via the production of adenosine; however, very little is known about CD73 expression in other immune cell populations that infiltrate the TME. The limited number of studies that have investigated the involvement of CD73 on MDSC-mediated immunosuppression is largely focused on the effects of this enzyme in G-MDSCs (*39*–*42*). Our study now shows that tumor-derived PGE_2 sustains M-MDSCs′ suppressive activity in a CD73-dependent manner but does not affect CD73 expression on G-MDSCs. The molecular mechanisms involved in the regulation of the CD73 ectonucleotidase are not well understood. Previously published reports have focused solely on the transcription factor Stat3 (*43*, *44*). Our data suggest a previously undescribed signaling pathway regulating CD73 expression in M-MDSCs that involves both the transcription factors Stat3 and CREB (Fig. 8).

This signaling pathway is initiated by tumor-derived PGE_2 that transduces intracellular signals through the EP2 receptor on M-MDSCs and involves a potential IL-6–dependent feed-forward loop activating Stat3, which together with cAMP → PKA–activated CREB, induces maximal CD73 expression (Fig. 8). This rational conclusion for this signaling pathway is supported by the fact that the CD73 promoter is strongly predicted to contain binding sites for both Stat3 and CREB, as determined by MatInspector, a software tool that uses a large library of matrix descriptions for transcription factor binding sites to accurately locate sites within DNA sequences to which transcription factors can bind (www.bioz.com/result/matinspector%20software%20tool/product/Genomatix). The increased CD73 expression on M-MDSCs results in an increased accumulation of adenosine in the TME, which ultimately suppresses antitumor T cell activity. We believe that there is no PGE_2 feed-forward loop in MDSCs since exogenous PGE_2 induces IL-10 expression which down-regulates COX-2 (*45*, *46*), and COX-2 is required for PGE_2 synthesis (*47*). The expression of CD73 is sustained by the exposure of the M-MDSCs to the continuous supply of tumor cell–derived PGE_2 in the TME.

Our data suggest that circulating $CD14^+$ monocytes from patients with NSCLC lack CD73 expression on their cell surface. It

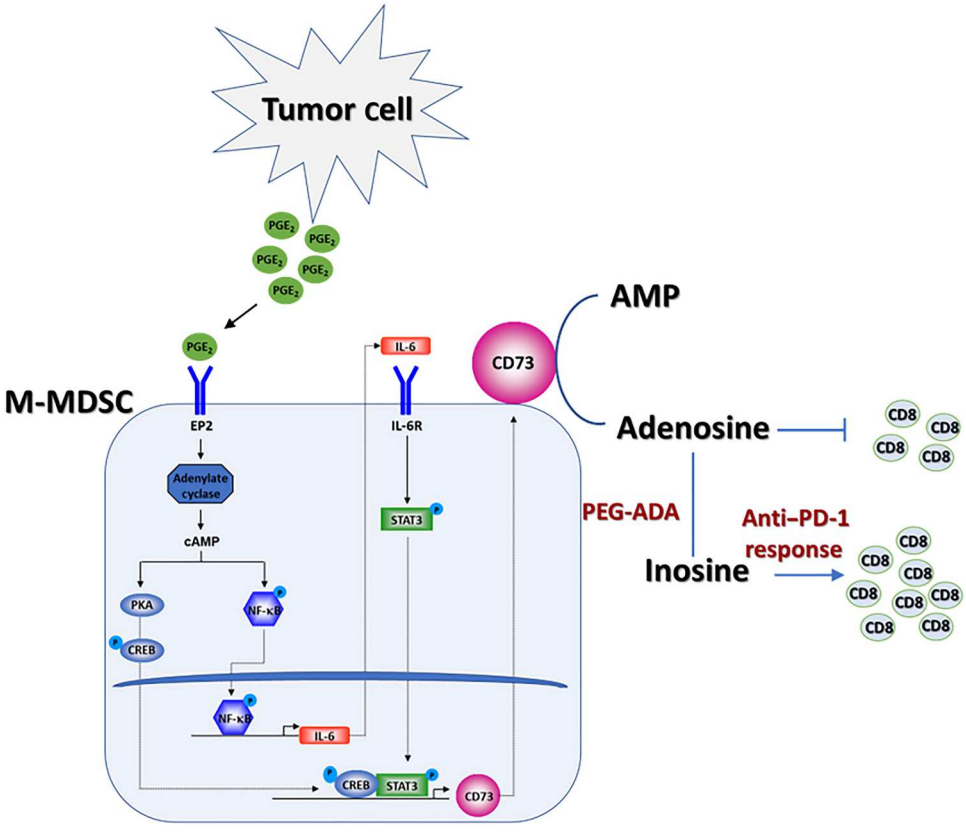

Fig. 8. Model of the proposed mechanism of M-MDSC–suppressive activity. Tumor-derived PGE_2 initiates a signaling cascade in M-MDSCs resulting in Stat3/CREB-dependent up-regulation of CD73 expression, inducing increased levels of adenosine in the TME culminating in the inhibition of antitumor T cell activity, and thus limits the efficacy of immunotherapy. Depletion of adenosine with PEG-ADA will overcome adenosine-mediated immunosuppression and sensitize tumors to immunotherapy.

is possible that CD73 expression could be up-regulated in these circulating monocytes upon their infiltration into the PGE_2-enriched TME. These data also highlight the diversity in the effector functions of circulating and tumor-infiltrating myeloid cells. Intriguingly, high levels of soluble CD73 in the blood have been shown to correlate with poor prognosis in metastatic cancer patients (*48*). CD73 is an enzyme that hydrolyzes extracellular AMP when expressed on the cell surface; however, there is a possibility that tumor-educated M-MDSCs present in the TME can shed CD73 protein into the extracellular milieu. Alternatively, MDSCs have been shown to secrete exosomes (*49*) which could be loaded with CD73 molecules. These possibilities remain to be explored. Our results also indicate that human M-MDSCs express CD73 but not CD39; this is in contrast with that observed in murine M-MDSCs, which express both CD39 and CD73 ectoenzymes. These data reiterate the previously observed differences between mouse and human MDSCs (*50*–*52*) and provide additional evidence that despite the phenotypic diversity, a similar PGE_2-induced molecular program controls the CD73-adenosine immunoregulatory axis in both human and murine M-MDSCs.

Targeting adenosine-mediated immune suppression is a focus of several ongoing clinical trials, the results from which are still anticipated. These include the use of an A2AR antagonist (CPI-444) administered either alone or with anti–PD-L1 (programmed death-ligand 1) (*53*) and humanized anti-CD73 antibodies CPI-006 and IPH5301 (clinical trials NCT03454451 and NCT05143970, respectively). We tested our immunotherapeutic strategy involving the administration of ADA, a highly efficacious, long-lasting, and nontoxic adenosine-depleting enzyme. The use of ADA represents a unique and highly clinically relevant approach to disengage adenosine-mediated T cell immune suppression and overcome anti–PD-1 therapeutic resistance in patients with cancer. ADA will not only eliminate the adenosine present in the TME but also convert it to inosine, which can be used by T cells as an energy source to support their effector functions in a glucose-deprived TME (*54*, *55*). Inosine has been shown to enhance the efficacy of immunotherapy by activating antitumor T cells in an A2AR-dependent manner in mouse models of cancer (*55*). The PEGylated version of ADA (PEG-ADA) is an FDA-approved biologic that is currently used as an enzyme replacement therapy for ADA deficiency in pediatric SCID patients. The attachment of PEG to the ADA molecule slows the clearance of ADA, increases the circulation half-life, and lowers binding by host antibodies, thus reducing toxicity (*56*). PEG-ADA enzyme can effectively eliminate the end-product of all the CD73 nucleotidase activity, i.e., adenosine, in the TME and thus can be more efficacious in targeting both intrinsic and acquired therapeutic resistance to anti–PD-1 Ab when compared to that offered by CD73-targeting antibodies (Fig. 8).

There are certain limitations to our study. It is unclear whether KP tumor regression in response to the PEG-ADA/anti–PD-1 combination therapy was $CD73^+$ MDSC-dependent. In addition, we were not able to formally determine the specific contribution of $CD73^+$ M-MDSCs to the total accumulated adenosine levels in the TME. Both of these limitations will be addressed in future studies using genetic deletion of CD73 specifically in M-MDSCs. Last, our murine studies are limited to orthotopic primary tumor settings and lack information regarding metastatic disease settings which will be investigated in future studies using multiple tumor models.

In summary, PGE_2 produced by tumor cells regulates CD73 expression in M-MDSCs via a Stat3 and CREB-dependent pathway resulting in increased extracellular adenosine generation that suppresses $CD8^+$ T cell activation in solid tumors. Furthermore, enzymatic depletion of extracellular adenosine reverses $CD8^+$ T cell exhaustion and sensitizes tumors to anti–PD-1 therapy.

MATERIALS AND METHODS

Patient samples

De-identified tumor and adjacent normal tissues and peripheral blood were collected from 18 patients with stage II/III NSCLC. Patients with NSCLC included in this study were not undergoing therapy when their samples were collected. Fresh tumor tissues were processed into single-cell suspensions for phenotype and functional studies or flash-frozen for adenosine measurements.

Study approvals

(i) NSCLC patient samples were collected after informed consent was obtained by the staff of the University of Louisville (UofL) Health-Cancer Center Biorepository and covered under the University of Louisville IRB protocol number 08.0388. (ii) Mice: All mice were handled in accordance with the Association for Assessment and Accreditation of Laboratory Animals Care international guidelines, with the approval of the Institutional Animal Care and Use Committee (IACUC) at the University of Louisville. The University of Louisville IACUC reviewed and approved this study under ID no. 21972.

Cell lines

The human melanoma cell line A375 [American Type Culture Collection (ATCC) CRL-1619], human lung cancer line A549 (ATCC CCL-185), mouse melanoma line B16-F10 (ATCC CRL 6475), mouse lung cancer line LLC (ATCC CRL-1642), and mouse breast cancer cell line 4T1 (ATCC CRL-2539) were purchased from ATCC (Manassas, VA) and maintained in Dulbecco's modified Eagle's medium (Corning) or RPMI 1640 (Corning) media containing 10% (v/v) fetal bovine serum (FBS). KP1.9 cells were obtained from Zippelius' lab. 4T1-sh*PTGES* and 4T1-shScr were generated by stable induction of lentiviral particles containing expression constructs for sh*PTGES* or Scr control, respectively (Origene Technologies) and selection in puromycin. Cells were frozen at passage two after receiving them from ATCC and were maintained in culture for no longer than 6 to 8 weeks. All cell lines were authenticated by the ATCC cell bank using the short tandem repeat profiling.

Biochemical reagents

Human and murine GM-CSF, IL-6, IL-4, and IL-10 were obtained from Peprotech. PGE_2 and D-cAMP were obtained from Tocris. The EP2 receptor agonist Butaprost and EP4 receptor agonist CAY10598 were obtained from Cayman. Forskolin was obtained from Enzo Life Sciences. STAT3 inhibitor S3I-201 and CREB inhibitor 666-15 were obtained from Calbiochem. Adenosine, ADA, AMP, AMP-CP, erythro-9-(2-hydroxy-3-nonyl) adenine (ADA inhibitor), OVA, and human serum were obtained from Sigma-Aldrich. Neutralizing anti–IL-10 Ab was obtained from R&D Systems. Carboxyfluorescein succinimidyl ester (CFSE) was obtained from Thermo Fisher Scientific.

Mice

Wild-type C57BL/6J and BALB/c, OT-I TCR transgenic, and *Nt5e*$^{-/-}$ C57BL/6 mice were purchased from The Jackson Laboratory. Mice were bred and housed in a pathogen-free barrier animal facility and maintained on a standard 12-hour light/12-hour dark cycle.

In vivo tumor experiments

Implantable tumor models

Syngeneic male 6- to 8-week-old C57BL/6 mice were inoculated subcutaneously with 2×10^5 LLC, B16-F10, or KP1.9 cells. Male mice were chosen for all these models since it has been reported that M-MDSCs are enriched in tumors from males compared to females in other cancer types (*57*). Female 6- to 8-week-old Balb/c mice were inoculated s.c with 2×10^5 4T1-shScr control cells or 4T1-*shPTGES* cells in the left flank.

Orthotopic NSCLC and breast cancer models

Confluent KP1.9 lung adenocarcinoma cells were detached with trypsin to obtain single-cell suspensions. A total of 0.5×10^6 KP1.9 cells were injected in the tail vein of 8- to 10-week-old wild-type C57BL/6 or *Nt5e*$^{-/-}$ C57BL/6 mice. For the breast cancer model, 4T1 mammary carcinoma cells were detached with trypsin to obtain single-cell suspensions. A total of 2.0×10^5 4T1 cells were directly inoculated in the mammary fat pads under anesthesia.

Tumor monitoring

(i) Subcutaneous tumor growth was monitored every 2 days using digital calipers to measure both the longitudinal and transverse diameters (in millimeters). Tumor-bearing mice were euthanized when tumors reached a volume of 2000 mm^3 or earlier if tumors ulcerated or animals showed signs of discomfort; (ii) orthotopic lung tumor growth was monitored using microcomputed tomography (CT) imaging using a MicroCAT II scanner (Siemens). Mice were anesthetized with isoflurane during the entire imaging procedure. Imaging was started at day 24 posttumor inoculation and continued once a week until day 42; and (iii) for histological analysis of tumor-bearing lung tissues, tissue sections of the lungs were prepared as previously described, with minor modifications (*58*). Briefly, before organ collection, intracardiac perfusion was performed with ice-cold PBS, and lung tissues were fixed in 10% neutral phosphate-buffered formalin for 24 hours at room temperature. After the tissues were embedded in paraffin blocks, paraffin microtomy (RM2135; Leica Biosystems) was performed at 5-μm thickness per section. To stain with hematoxylin (95057-844; VWR, Radnor, PA) and eosin (HT110232; Thermo Fisher Scientific), sections were deparaffinized and rehydrated in xylene, ethanol, and deionized water and stained (*58*). Stained slides were dehydrated with ethanol, which was then extracted with xylene. Xylene-based Permount mounting medium (SP15-500; Thermo Fisher Scientific, Waltham, MA) was used to affix the coverslips to the slide. Slides were scanned using an Aperio Imagescope (Leica Biosystems).

Treatment of tumor-bearing mice

(i) PEG-ADA monotherapy—KP1.9 NSCLC cells or 4T1 cells were injected at 2×10^5 cells per mouse. Two groups of KP1.9-bearing mice (n = 20 mice per group) or orthotopic 4T1-bearing mice (n = 10 mice per group) received the following treatments every other day via the intraperitoneal route: 1) vehicle control (saline) and 2) PEG-ADA (2 U per mouse; procured from Leadiant Biosciences, Gaithersburg, MD, USA). Tumors were measured by digital calipers and plotted as volume/time; and (ii) PEG-ADA and anti–PD-1 combination therapy—Four groups of KP1.9-bearing mice (n = 8 mice per group) received the following treatments starting either at day 0 or day 7 and then every other day via the intraperitoneal route: 1) vehicle control (saline), 2) anti–PD-1 Ab alone (clone RMPI-14, 250 μg per mouse, Bio X Cell), 3) PEG-ADA alone (2 U per mouse), and 4) anti–PD-1 plus PEG-ADA.

Endpoints for experiments with mice were selected in accordance with institutional-approved criteria. All tumor cell lines used in the in vivo experiments were routinely tested for mycoplasma contamination using a Mycoalert plus mycoplasma detection kit (Lonza). Randomization of animals was not used in experiments, and no blinding was done for the animal experiments.

In vitro generation of human and murine M-MDSCs

(i) To generate tumor cell line–induced human M-MDSCs, CD14$^+$ cells (1×10^6) isolated from peripheral blood mononuclear cells (PBMCs) obtained from healthy donors were cocultured with A375 or A549 tumor cells (5×10^5) in complete Iscove's modified Dulbecco's medium (IMDM) medium (IMDM + 10% human serum) per well in a six-well Transwell system separated by a 0.4-μm membrane. A375 and A549 cocultured monocytes and control monocytes cultured without tumor cells were harvested from the bottom wells by gently scraping after 68 to 72 hours of culture; (ii) to generate PGE_2-induced human M-MDSCs, CD14$^+$ cells (1×10^6) isolated from PBMCs obtained from healthy donors were treated with GM-CSF (10 ng/ml) and PGE_2 (1 μM) for 6 days. Half of the culture medium was replaced with fresh medium containing GM-CSF/PGE_2 every 48 hours. In some experiments, Butaprost (10 μM) and CAY10598 (10 nM) were added at the beginning of the 6-day culture; and (iii) to generate murine PGE_2-induced M-MDSCs, fresh BM cells were harvested from the tibia and femur of C57BL/6 mice using a previously established protocol (*9*). BM cells were cultured for 5 days in complete RPMI medium (RPMI + 10% FBS/10 mM Hepes/20 μM 2-Mercaptoethanol (BME)) with murine GM-CSF (20 ng/ml) and PGE_2 (2.6 μM). Half of the medium was replaced every 48 hours with fresh BM medium containing GM-CSF/PGE_2. In some experiments, BM cells were cultured with GM-CSF alone (20 ng/ml) or GM-CSF/PGE_2 (2.6 μM) in the presence of either vehicle control (dimethyl sulfoxide) or STAT3 inhibitor (S3I-201; 100 μM, added every 24 hours) or CREB inhibitor (666-15; 1 μM, added once) for 72 hours. Half of the medium was replaced every 48 hours with fresh BM medium containing GM-CSF/PGE_2.

In vivo transfer of M-MDSCs

BM cells were harvested from both wild-type and *Nt5e*$^{-/-}$ mice, and PGE_2-induced M-MDSCs were generated as mentioned above. M-MDSCs were sorted from day 5 BM cultures, and the purified M-MDSCs (2×10^5) were mixed with KP1.9 cells (1.5×10^5) in 200 μl of PBS and injected subcutaneously into wild-type C57BL/6 and *Nt5e*$^{-/-}$ mice (n = 7 mice per group). Tumor growth was measured using digital calipers. For adoptive transfer experiments, 0.5×10^6 KP1.9 cells were injected in the tail vein of 8- to 10-week-old wild-type C57BL/6 and *Nt5e*$^{-/-}$ C57BL/6 mice. Lungs from tumor-bearing mice were processed into single-cell suspensions, and CD11b^{hi}Gr-1^{int} M-MDSCs were purified. Wild-type (C57BL/6) or *Nt5e*$^{-/-}$ mice that were injected subcutaneously with KP1.9 tumor cells (1.5×10^5) mixed with either wild-type or *Nt5e*$^{-/-}$ M-MDSCs

(2×10^5) ($n = 5$ in each group). Tumor growth was measured using digital calipers.

In vitro generation of human and murine DCs

(i) To generate human monocyte-derived DCs, $CD14^+$ cells (1×10^6) isolated from PBMCs obtained from healthy donors were treated with GM-CSF (10 ng/ml) and IL-4 (10 ng/ml) for 6 days. Half of the culture medium was replaced with fresh medium containing GM-CSF/IL-4 every 48 hours; and (ii) to generate murine DCs, BM cells were cultured for 5 days in complete RPMI medium with murine GM-CSF (40 ng/ml) and IL-4 (10 ng/ml). Half of the medium was replaced every 48 hours with fresh BM medium containing GM-CSF/IL-4.

Isolation of murine lung mononuclear cells

Lung mononuclear cells (LMCs) were isolated as described previously with modifications (*59*). Briefly, single-cell suspensions were prepared first by cutting lungs into ~1-mm segments, followed by incubation at 37°C for 30 min in RPMI 1640 with Liberase (50 μg/ml) and deoxyribonuclease I (1 μg/ml). An isotonic discontinuous Percoll (GE Healthcare) density gradient [30:70% (v/v)] was then used for mononuclear cell isolation.

M-MDSC isolation

(i) Human $CD14^+CD73^+$ tumor–associated monocytes were positively selected from human NSCLC lesions. Fresh tumor tissues from patients with NSCLC were enzymatically digested, and single-cell suspensions were stained with CD14 microbeads (Miltenyi Biotec) and positively selected using AutoMACS ProSeparator (Miltenyi Biotec). $CD14^+$ cells were then stained with biotinylated antihuman CD73 Ab and streptavidin microbeads, and $CD14^+CD73^+$ cells were separated using AutoMACS ProSeparator; and (ii) murine $CD11b^+Gr\text{-}1^{int}$ M-MDSCs were positively selected from PGE_2-induced BM-MDSCs and from LMCs obtained from naïve, KP1.9-bearing wild-type and *Nt5e* $^{-/-}$ mice using the murine MDSC isolation kit (Miltenyi Biotec). For purifying $CD73^+$ and $CD73^{neg}$ murine M-MDSCs, purified M-MDSC cells were stained with biotinylated anti-mouse CD73 Ab and streptavidin microbeads and were sorted using the AutoMACS Pro Separator.

Flow cytometry analysis

For surface staining, single-cell suspensions were washed and resuspended in PBS and stained with Fixable Viability Dye eFluor 450 (Thermo Fisher Scientific, USA) for 15 min. Cells were then washed twice and resuspended in flow cytometry buffer (2% FBS + PBS) and stained with multicolor Ab cocktails according to the manufacturer′s recommendations. Antibodies used in this study are provided in table S1. Murine cells were incubated with CD16/CD32 Ab (2.4G2) for 10 min at 4°C to block Fc receptors before being stained for surface markers. For intracellular staining, cells were fixed in Fix/Perm solution [Becton Dickinson (BD) Biosciences]. After being washed with Perm/Wash buffer (BD Biosciences), the cells were stained intracellularly for 30 min, washed, and resuspended in flow buffer. Stained cells were analyzed with a FACSCanto II (BD Biosciences, Franklin Lakes, NJ), and data were analyzed using FlowJo v10 (BD Biosciences, Franklin Lakes, NJ). Dot plots are represented with log-scale axes. Histograms are represented on a log-scale *x-axis* and a linear *y-axis*.

Immunosuppressive assays

The suppressive function of human and murine M-MDSCs was performed using our previously established protocol (*9*). For human M-MDSC–suppressive assays, autologous T cells were isolated from patient NSCLC lesions or from healthy donor PBMCs using the Pan T cell Isolation Kit (Miltenyi Biotec). Autologous T cells were cocultured with either (i) $CD14^+CD73^+$ cells from patient tumors, (ii) A375/A549 cell line–induced M-MDSCs, (iii) PGE_2-induced M-MDSCs, (iv) $CD73^+$ and $CD73^{neg}$ M-MDSCs, or (v) $CD73^+$ MDSC–derived supernatants that were untreated or treated with ADA. Cultures were then stimulated with either anti-CD3 and anti-CD28 antibodies or tetanus toxoid (1.0 μg/ml) (in 96-well flat-bottomed plates) or anti-CD3/anti-CD28 beads (in 96-well round-bottomed plates) for 4 or 5 days. T cell proliferation was measured by $^{[3H]}$thymidine incorporation. For analysis of proliferation with flow cytometry, (i) autologous T cells were prelabeled with CFSE (5 μM); and (ii) for murine M-MDSC–suppressive assays, splenocytes from OTI transgenic mice were cocultured with M-MDSCs from BM or KP1.9 tumor–bearing lungs at different ratios in the presence of OVA (250 μg/ml) for 4 days, and proliferation of $CD8^+$ T cells was measured. In some experiments, M-MDSCs were pretreated with CD73 inhibitor AMP-CP (10 μM) and AMP for 8 hours, and supernatants were added to T cells and proliferation was measured.

Quantitative PCR analysis

RNA was extracted from $CD14^+$ cells using the RNAeasy micro kit (Qiagen) following the manufacturer′s instructions. Reverse transcription was performed with the iScript cDNA synthesis kit (Bio-Rad). Quantitative mRNA assessment was performed by real-time reverse transcription PCR using TaqMan Universal Master Mix (Applied Biosystems) as previously described (*9*, *60*). The following TaqMan probes from Applied Biosystems were used according to the manufacturer′s instructions: 18s (Hs99999901_s1; VIC), CD73 (Hs00159686_m1; FAM), CD39 (Hs00969559_m1), IL-6 (Hs00174131_m1; FAM), IL-10 (Hs00961619_m1; FAM), and A2AR (Hs00169123_m1; FAM).

Enzyme-linked immunosorbent assay

PGE_2 was measured by ELISA (R&D Systems) in supernatants from murine LLC, KP1.9, and B16-F10 cell cultures. IL-10 levels were measured by ELISA in supernatants from human $CD14^+$ monocytes. A human IL-10 ELISA kit was obtained from R&D Systems.

Adenosine measurement

Adenosine in tumors from patients with NSCLC and in M-MDSC culture supernatants was measured by liquid chromatography coupled with tandem mass spectrometry. Adenosine was measured in fresh culture supernatants of CD73–M-MDSCs treated with AMP (10 μM) for 6 to 8 hours, and erythro-9-(2-hydroxy-3-nonyl) adenine, an inhibitor of ADA, was added to the culture supernatant to prevent adenosine degradation over time. One milligram of tumor tissue was homogenized in 25 μl of 80% methanol (MeOH). Gentle N_2 flow was applied to evaporate the MeOH. Freeze-fried samples were reconstituted with 400 μl of water, and 2 μl of the injection volume was used for LC-MS analysis. The linear range for adenosine quantification on an LC-MS instrument was determined as 50 to 50,000 nM. The multiple reaction monitoring method was applied to qualify and quantify adenosine.

Immunoblotting

$CD14^+$ cells were cultured in complete IMDM (IMDM + 10% human serum) and were treated with GM-CSF alone (10 ng/ml) or GM-CSF/PGE_2 (1 μM), GM-CSF/IL-6 (10 ng/ml), Forskolin (10 μM), D-cAMP (100 μM), STAT3 inhibitor (S3I-201; 100 μM), CREB inhibitor (666-15; 2 μM), and STAT3i/CREBi combination. Cells were lysed in radioimmunoprecipitation assay buffer (Sigma-Aldrich) supplemented with a protease inhibitor cocktail (Sigma-Aldrich) and 10 mM $NaV0_4$, and equal amounts of proteins were analyzed by Western blot using a NuPage Novex gel system (Thermo Fisher Scientific) using the following antibodies: from Cell Signaling Technology: Phospho-Stat3 (Tyr^{705}; 9138), Stat3 (9139), phospho–NF-κB (Ser^{536}; 3033), NF-κB (8242), IκBα (9242), phospho-CREB (Ser^{133}; 9198), and CREB (9197); and from Santa Cruz Biotechnology: PTGES (sc365844). For signaling studies in murine MDSCs, BM cells were cultured for 0, 16, 24, 48, 72, and 96 hours in complete RPMI medium (RPMI + 10% FBS/10 mM Hepes/20 μM BME) with either murine GM-CSF (20 ng/ml) alone or GM-CSF and PGE_2 (2.6 μM). Half of the medium was replaced every 48 hours with fresh BM medium containing GM-CSF/PGE_2. Cells were lysed and immunoblotted as described above.

Statistical analysis

GraphPad Prism 8.0 software (GraphPad Prism Software Inc., La Jolla, CA) and SAS version 9.4 (SAS Institute Inc., Cary, NC) were used for statistical analyses. Two-group comparisons between control and test samples (groups compared are indicated in the respective figures) were done by two-tailed Student's *t-tests*. Multiple data comparisons were derived by one-way analysis of variance (ANOVA) followed by Tukey's post hoc test. Correlations between PGE_2 levels and $CD73^+$ M-MDSC frequencies were assessed using Spearman's rank correlation. For all tests, statistical significance was assumed where $P < 0.05$. For all figures, $^*P < 0.05$, $^{**}P < 0.005$, and $^{***}P < 0.0005$.

Supplementary Materials

This PDF file includes:

Figs. S1 to S4

Table S1

View/request a protocol for this paper from *Bio-protocol*.

REFERENCES AND NOTES

1. S. N. Gettinger, L. Horn, L. Gandhi, D. R. Spigel, S. J. Antonia, N. A. Rizvi, J. D. Powderly, R. S. Heist, R. D. Carvajal, D. M. Jackman, L. V. Sequist, D. C. Smith, P. Leming, D. P. Carbone, M. C. Pinder-Schenck, S. L. Topalian, F. S. Hodi, J. A. Sosman, M. Sznol, D. F. McDermott, D. M. Pardoll, V. Sankar, C. M. Ahlers, M. Salvati, J. M. Wigginton, M. D. Hellmann, G. D. Kollia, A. K. Gupta, J. R. Brahmer, Overall survival and long-term safety of nivolumab (Anti-programmed death 1 antibody, BMS-936558, ONO-4538) in patients with previously treated advanced non-small-cell lung cancer. *J. Clin. Oncol.* **33**, 2004–2012 (2015).
2. S. L. Topalian, C. G. Drake, D. M. Pardoll, Immune checkpoint blockade: A common denominator approach to cancer therapy. *Cancer Cell* **27**, 450–461 (2015).
3. M. Yarchoan, A. Hopkins, E. M. Jaffee, Tumor mutational burden and response rate to PD-1 inhibition. *N. Engl. J. Med.* **377**, 2500–2501 (2017).
4. N. A. Rizvi, M. D. Hellmann, A. Snyder, P. Kvistborg, V. Makarov, J. J. Havel, W. Lee, J. Yuan, P. Wong, T. S. Ho, M. L. Miller, N. Rekhtman, A. L. Moreira, F. Ibrahim, C. Bruggeman, B. Gasmi, R. Zappasodi, Y. Maeda, C. Sander, E. B. Garon, T. Merghoub, J. D. Wolchok, T. N. Schumacher, T. A. Chan, Cancer immunology. Mutational landscape determines sensitivity to PD-1 blockade in non-small cell lung cancer. *Science* **348**, 124–128 (2015).
5. N. McGranahan, A. J. Furness, R. Rosenthal, S. Ramskov, R. Lyngaa, S. K. Saini, M. Jamal-Hanjani, G. A. Wilson, N. J. Birkbak, C. T. Hiley, T. B. Watkins, S. Shafi, N. Murugaesu, R. Mitter, A. U. Akarca, J. Linares, T. Marafioti, J. Y. Henry, E. M. Van Allen, D. Miao, B. Schilling, D. Schadendorf, L. A. Garraway, V. Makarov, N. A. Rizvi, A. Snyder, M. D. Hellmann, T. Merghoub, J. D. Wolchok, S. A. Shukla, C. J. Wu, K. S. Peggs, T. A. Chan, S. R. Hadrup, S. A. Quezada, C. Swanton, Clonal neoantigens elicit T cell immunoreactivity and sensitivity to immune checkpoint blockade. *Science* **351**, 1463–1469 (2016).
6. A. Gros, M. R. Parkhurst, E. Tran, A. Pasetto, P. F. Robbins, S. Ilyas, T. D. Prickett, J. J. Gartner, J. S. Crystal, I. M. Roberts, K. Trebska-McGowan, J. R. Wunderlich, J. C. Yang, S. A. Rosenberg, Prospective identification of neoantigen-specific lymphocytes in the peripheral blood of melanoma patients. *Nat. Med.* **22**, 433–438 (2016).
7. V. Kumar, S. Patel, E. Tcyganov, D. I. Gabrilovich, The nature of myeloid-derived suppressor cells in the tumor microenvironment. *Trends Immunol.* **37**, 208–220 (2016).
8. S. Ostrand-Rosenberg, C. Fenselau, Myeloid-derived suppressor cells: Immune-suppressive cells that impair antitumor immunity and are sculpted by their environment. *J. Immunol.* **200**, 422–431 (2018).
9. K. Yaddanapudi, B. E. Rendon, G. Lamont, E. J. Kim, N. Al Rayyan, J. Richie, S. Albeituni, S. Waigel, A. Wise, R. A. Mitchell, MIF is necessary for late-stage melanoma patient MDSC immune suppression and differentiation. *Cancer Immunol. Res.* **4**, 101–112 (2016).
10. I. Marigo, E. Bosio, S. Solito, C. Mesa, A. Fernandez, L. Dolcetti, S. Ugel, N. Sonda, S. Bicciato, E. Falisi, F. Calabrese, G. Basso, P. Zanovello, E. Cozzi, S. Mandruzzato, V. Bronte, Tumor-induced tolerance and immune suppression depend on the C/EBPbeta transcription factor. *Immunity* **32**, 790–802 (2010).
11. E. K. Vetsika, F. Koinis, M. Gioulbasani, D. Aggouraki, A. Koutoulaki, E. Skalidaki, D. Mavroudis, V. Georgoulias, A. Kotsakis, A circulating subpopulation of monocytic myeloid-derived suppressor cells as an independent prognostic/predictive factor in untreated non-small lung cancer patients. *J. Immunol. Res.* **2014**, 659294 (2014).
12. D. Marvel, D. I. Gabrilovich, Myeloid-derived suppressor cells in the tumor microenvironment: Expect the unexpected. *J. Clin. Invest.* **125**, 3356–3364 (2015).
13. B. Weide, A. Martens, H. Zelba, C. Stutz, E. Derhovanessian, A. M. Di Giacomo, M. Maio, A. Sucker, B. Schilling, D. Schadendorf, P. Buttner, C. Garbe, G. Pawelec, Myeloid-derived suppressor cells predict survival of patients with advanced melanoma: Comparison with regulatory T cells and NY-ESO-1- or melan-A-specific T cells. *Clin. Cancer Res.* **20**, 1601–1609 (2014).
14. Z. Wang, L. Zhang, H. Wang, S. Xiong, Y. Li, Q. Tao, W. Xiao, H. Qin, Y. Wang, Z. Zhai, Tumor-induced CD14+HLA-DR (−/low) myeloid-derived suppressor cells correlate with tumor progression and outcome of therapy in multiple myeloma patients. *Cancer Immunol. Immunother.* **64**, 389–399 (2015).
15. A. Ohta, M. Sitkovsky, Extracellular adenosine-mediated modulation of regulatory T cells. *Front. Immunol.* **5**, 304 (2014).
16. V. Umansky, I. Shevchenko, A. V. Bazhin, J. Utikal, Extracellular adenosine metabolism in immune cells in melanoma. *Cancer Immunol. Immunother.* **63**, 1073–1080 (2014).
17. S. Deaglio, K. M. Dwyer, W. Gao, D. Friedman, A. Usheva, A. Erat, J. F. Chen, K. Enjyoji, J. Linden, M. Oukka, V. K. Kuchroo, T. B. Strom, S. C. Robson, Adenosine generation catalyzed by CD39 and CD73 expressed on regulatory T cells mediates immune suppression. *J. Exp. Med.* **204**, 1257–1265 (2007).
18. A. Ohta, R. Kini, M. Subramanian, M. Madasu, M. Sitkovsky, The development and immunosuppressive functions of $CD4^+$ $CD25^+$ $FoxP3^+$ regulatory T cells are under influence of the adenosine-A2A adenosine receptor pathway. *Front. Immunol.* **3**, 190 (2012).
19. A. Ohta, M. Sitkovsky, Role of G-protein-coupled adenosine receptors in downregulation of inflammation and protection from tissue damage. *Nature* **414**, 916–920 (2001).
20. M. S. Hershfield, R. H. Buckley, M. L. Greenberg, A. L. Melton, R. Schiff, C. Hatem, J. Kurtzberg, M. L. Markert, R. H. Kobayashi, A. L. Kobayashi, A. Abuchowski, Treatment of adenosine deaminase deficiency with polyethylene glycol-modified adenosine deaminase. *N. Engl. J. Med.* **316**, 589–596 (1987).
21. D. Allard, B. Allard, P. O. Gaudreau, P. Chrobak, J. Stagg, CD73-adenosine: A next-generation target in immuno-oncology. *Immunotherapy* **8**, 145–163 (2016).
22. S. Narumiya, G. A. FitzGerald, Genetic and pharmacological analysis of prostanoid receptor function. *J. Clin. Invest.* **108**, 25–30 (2001).
23. X. Sun, Q. Li, Prostaglandin EP2 receptor: Novel therapeutic target for human cancers (Review). *Int. J. Mol. Med.* **42**, 1203–1214 (2018).
24. T. A. Libermann, D. Baltimore, Activation of interleukin-6 gene expression through the NF-kappa B transcription factor. *Mol. Cell. Biol.* **10**, 2327–2334 (1990).
25. H. L. Pahl, Activators and target genes of Rel/NF-κB transcription factors. *Oncogene* **18**, 6853–6866 (1999).
26. J. Takeda, K. Adachi, K. M. Halprin, S. Itami, V. Levine, C. Woodyard, Forskolin activates adenylate cyclase activity and inhibits mitosis in in vitro in pig epidermis. *J. Invest. Dermatol.* **81**, 236–240 (1983).

27. K. B. Seamon, J. W. Daly, Forskolin: Its biological and chemical properties. *Adv. Cyclic Nucleotide Protein Phosphorylation Res.* **20**, 1–150 (1986).
28. E. M. Abd-El-Basset, M. S. Rao, Dibutyryl cyclic adenosine monophosphate rescues the neurons from degeneration in stab wound and excitotoxic injury models. *Front. Neurosci.* **12**, 546 (2018).
29. T. Tanaka, M. Narazaki, T. Kishimoto, IL-6 in inflammation, immunity, and disease. *Cold Spring Harb. Perspect. Biol.* **6**, a016295 (2014).
30. H. Zhang, Q. Kong, J. Wang, Y. Jiang, H. Hua, Complex roles of cAMP-PKA-CREB signaling in cancer. *Exp. Hematol. Oncol.* **9**, 32 (2020).
31. P. Sinha, V. K. Clements, A. M. Fulton, S. Ostrand-Rosenberg, Prostaglandin E2 promotes tumor progression by inducing myeloid-derived suppressor cells. *Cancer Res.* **67**, 4507–4513 (2007).
32. M. DuPage, A. F. Cheung, C. Mazumdar, M. M. Winslow, R. Bronson, L. M. Schmidt, D. Crowley, J. Chen, T. Jacks, Endogenous T cell responses to antigens expressed in lung adenocarcinomas delay malignant tumor progression. *Cancer Cell* **19**, 72–85 (2011).
33. R. Hirschhorn, F. Martiniuk, F. S. Rosen, Adenosine deaminase activity in normal tissues and tissues from a child with severe combined immunodeficiency and adenosine deaminase deficiency. *Clin. Immunol. Immunopathol.* **9**, 287–292 (1978).
34. A. Cohen, R. Hirschhorn, S. D. Horowitz, A. Rubinstein, S. H. Polmar, R. Hong, D. W. Martin Jr., Deoxyadenosine triphosphate as a potentially toxic metabolite in adenosine deaminase deficiency. *Proc. Natl. Acad. Sci. U.S.A.* **75**, 472–476 (1978).
35. J. E. Talmadge, D. I. Gabrilovich, History of myeloid-derived suppressor cells. *Nat. Rev. Cancer* **13**, 739–752 (2013).
36. D. I. Gabrilovich, S. Nagaraj, Myeloid-derived suppressor cells as regulators of the immune system. *Nat. Rev. Immunol.* **9**, 162–174 (2009).
37. R. Weber, V. Fleming, X. Hu, V. Nagibin, C. Groth, P. Altevogt, J. Utikal, V. Umansky, Myeloid-derived suppressor cells hinder the anti-cancer activity of immune checkpoint inhibitors. *Front. Immunol.* **9**, 1310 (2018).
38. M. Delaunay, N. Guibert, A. Lusque, M. Farella, N. Boubekeur, S. Gouin, I. Dormoy, P. Fons, M. Esquerre, G. Favre, A. Pradines, J. Mazieres, Baseline circulating myeloid-derived suppressor cells and response to PD-1 inhibitor in non-small cell lung cancer patients. *J. Clin. Oncol.* **36**, 145–145 (2018).
39. E. Limagne, R. Euvrard, M. Thibaudin, C. Rebe, V. Derangere, A. Chevriaux, R. Boidot, F. Vegran, N. Bonnefoy, J. Vincent, L. Bengrine-Lefevre, S. Ladoire, D. Delmas, L. Apetoh, F. Ghiringhelli, Accumulation of MDSC and Th17 cells in patients with metastatic colorectal cancer predicts the efficacy of a FOLFOX-bevacizumab drug treatment regimen. *Cancer Res.* **76**, 5241–5252 (2016).
40. S. Ryzhov, S. V. Novitskiy, A. E. Goldstein, A. Biktasova, M. R. Blackburn, I. Biaggioni, M. M. Dikov, I. Feoktistov, Adenosinergic regulation of the expansion and immunosuppressive activity of $CD11b^{+}Gr1^{+}$ cells. *J. Immunol.* **187**, 6120–6129 (2011).
41. S. V. Ryzhov, M. W. Pickup, A. Chytil, A. E. Gorska, Q. Zhang, P. Owens, I. Feoktistov, H. L. Moses, S. V. Novitskiy, Role of TGF-β signaling in generation of $CD39^{+}CD73^{+}$ myeloid cells in tumors. *J. Immunol.* **193**, 3155–3164 (2014).
42. W. Hou, P. Sampath, J. J. Rojas, S. H. Thorne, Oncolytic virus-mediated targeting of PGE2 in the tumor alters the immune status and sensitizes established and resistant tumors to immunotherapy. *Cancer Cell* **30**, 108–119 (2016).
43. S. Y. Neo, Y. Yang, J. Record, R. Ma, X. Chen, Z. Chen, N. P. Tobin, E. Blake, C. Seitz, R. Thomas, A. K. Wagner, J. Andersson, J. de Boniface, J. Bergh, S. Murray, E. Alici, R. Childs, M. Johansson, L. S. Westerberg, F. Haglund, J. Hartman, A. Lundqvist, CD73 immune checkpoint defines regulatory NK cells within the tumor microenvironment. *J. Clin. Invest.* **130**, 1185–1198 (2020).
44. F. Chalmin, G. Mignot, M. Bruchard, A. Chevriaux, F. Vegran, A. Hichami, S. Ladoire, V. Derangere, J. Vincent, D. Masson, S. C. Robson, G. Eberl, J. R. Pallandre, C. Borg, B. Ryffel, L. Apetoh, C. Rebe, F. Ghiringhelli, Stat3 and Gfi-1 transcription factors control Th17 cell immunosuppressive activity via the regulation of ectonucleotidase expression. *Immunity* **36**, 362–373 (2012).
45. H. Niiro, T. Otsuka, T. Tanabe, S. Hara, S. Kuga, Y. Nemoto, Y. Tanaka, H. Nakashima, S. Kitajima, M. Abe, Y. Niho, Inhibition by interleukin-10 of inducible cyclooxygenase expression in lipopolysaccharide-stimulated monocytes: Its underlying mechanism in comparison with interleukin-4. *Blood* **85**, 3736–3745 (1995).
46. D. J. Berg, J. Zhang, D. M. Lauricella, S. A. Moore, Il-10 is a central regulator of cyclooxygenase-2 expression and prostaglandin production. *J. Immunol.* **166**, 2674–2680 (2001).
47. A. Greenhough, H. J. Smartt, A. E. Moore, H. R. Roberts, A. C. Williams, C. Paraskeva, A. Kaidi, The COX-2/PGE2 pathway: Key roles in the hallmarks of cancer and adaptation to the tumour microenvironment. *Carcinogenesis* **30**, 377–386 (2009).
48. S. Morello, M. Capone, C. Sorrentino, D. Giannarelli, G. Madonna, D. Mallardo, A. M. Grimaldi, A. Pinto, P. A. Ascierto, Soluble CD73 as biomarker in patients with metastatic melanoma patients treated with nivolumab. *J. Transl. Med.* **15**, 244 (2017).
49. C. Fenselau, S. Ostrand-Rosenberg, Molecular cargo in myeloid-derived suppressor cells and their exosomes. *Cell. Immunol.* **359**, 104258 (2021).
50. C. Vanhaver, P. van der Bruggen, A. M. Bruger, MDSC in mice and men: Mechanisms of immunosuppression in cancer. *J. Clin. Med.* **10**, 2872 (2021).
51. V. Bronte, S. Brandau, S. H. Chen, M. P. Colombo, A. B. Frey, T. F. Greten, S. Mandruzzato, P. J. Murray, A. Ochoa, S. Ostrand-Rosenberg, P. C. Rodriguez, A. Sica, V. Umansky, R. H. Vonderheide, D. I. Gabrilovich, Recommendations for myeloid-derived suppressor cell nomenclature and characterization standards. *Nat. Commun.* **7**, 12150 (2016).
52. L. Cassetta, E. S. Baekkevold, S. Brandau, A. Bujko, M. A. Cassatella, A. Dorhoi, C. Krieg, A. Lin, K. Lore, O. Marini, J. W. Pollard, M. Roussel, P. Scapini, V. Umansky, G. J. Adema, Deciphering myeloid-derived suppressor cells: Isolation and markers in humans, mice and non-human primates. *Cancer Immunol. Immunother.* **68**, 687–697 (2019).
53. L. Fong, P. M. Forde, J. D. Powderly, J. W. Goldman, J. J. Nemunaitis, J. J. Luke, M. D. Hellmann, S. Kummar, R. C. Doebele, D. Mahadevan, S. M. Gadgeel, B. G. M. Hughes, B. Markman, M. J. Riese, J. Brody, L. A. Emens, I. McCaffery, R. A. Miller, G. Laport, Safety and clinical activity of adenosine A2a receptor (A2aR) antagonist, CPI-444, in anti-PD1/PDL1 treatment-refractory renal cell (RCC) and non-small cell lung cancer (NSCLC) patients. *J. Clin. Oncol.* **35**, 3004–3004 (2017).
54. T. Wang, J. N. R. Gnanaprakasam, X. Chen, S. Kang, X. Xu, H. Sun, L. Liu, H. Rodgers, E. Miller, T. A. Cassel, Q. Sun, S. Vicente-Munoz, M. O. Warmoes, P. Lin, Z. L. Piedra-Quintero, M. Guerau-de-Arellano, K. A. Cassady, S. G. Zheng, J. Yang, A. N. Lane, X. Song, T. W. Fan, R. Wang, Inosine is an alternative carbon source for $CD8^{+}$-T-cell function under glucose restriction. *Nat. Metab.* **2**, 635–647 (2020).
55. L. F. Mager, R. Burkhard, N. Pett, N. C. A. Cooke, K. Brown, H. Ramay, S. Paik, J. Stagg, R. A. Groves, M. Gallo, I. A. Lewis, M. B. Geuking, K. D. McCoy, Microbiome-derived inosine modulates response to checkpoint inhibitor immunotherapy. *Science* **369**, 1481–1489 (2020).
56. S. Davis, A. Abuchowski, Y. K. Park, F. F. Davis, Alteration of the circulating life and antigenic properties of bovine adenosine deaminase in mice by attachment of polyethylene glycol. *Clin. Exp. Immunol.* **46**, 649–652 (1981).
57. D. Bayik, Y. Zhou, C. Park, C. Hong, D. Vail, D. J. Silver, A. Lauko, G. Roversi, D. C. Watson, A. Lo, T. J. Alban, M. McGraw, M. Sorensen, M. M. Grabowski, B. Otvos, M. A. Vogelbaum, C. Horbinski, B. W. Kristensen, A. M. Khalil, T. H. Hwang, M. S. Ahluwalia, F. Cheng, J. D. Lathia, Myeloid-derived suppressor cell subsets drive glioblastoma growth in a sex-specific manner. *Cancer Discov.* **10**, 1210–1225 (2020).
58. A. H. Fischer, K. A. Jacobson, J. Rose, R. Zeller, Hematoxylin and eosin staining of tissue and cell sections. *CSH Protoc* **2008**, pdb prot4986 (2008).
59. Q. Li, C. D. Anderson, N. K. Egilmez, Inhaled IL-10 Suppresses Lung Tumorigenesis via Abrogation of Inflammatory Macrophage-Th17 Cell Axis. *J. Immunol.* **201**, 2842–2850 (2018).
60. K. Yaddanapudi, K. Putty, B. E. Rendon, G. J. Lamont, J. D. Faughn, A. Satoskar, A. Lasnik, J. W. Eaton, R. A. Mitchell, Control of tumor-associated macrophage alternative activation by macrophage migration inhibitory factor. *J. Immunol.* **190**, 2984–2993 (2013).

Acknowledgments: We are grateful to Leadiant Biosciences (Gaithersburg, MD, USA) for providing PEG-ADA for this study. **Funding:** This work was supported by grants from the National Institutes of Health grant P20GM135004 (to K.Y. and J.A.C.) and the National Institutes of Health grant R21CA245560 (to K.Y.). **Author contributions:** K.Y., H.D., and J.E. conceived the experiments. O.S.S., H.D., N.A.R., L.C.C., and B.S. conducted the in vitro and in vivo experiments; X.Z. performed the metabolomics experiments; A.W. and C.L. performed the IHC experiments; M.H., R.A.M., A.Z., and J.C. provided reagents and resources; K.Y., O.S.S., and H.D. analyzed the results; K.Y. wrote the manuscript; H.D. and O.S.S. contributed and reviewed the manuscript; and O.S.S. and H.D. share co–first author position. The method used in assigning the authorship order among these authors is based on the time order in which they worked on this study. **Competing interests:** The authors declare that they have no competing interests. **Data and materials availability:** All data needed to evaluate the conclusions in the paper are present in the paper and/or the Supplementary Materials.

Submitted 19 December 2022
Accepted 26 May 2023
Published 30 June 2023
10.1126/sciadv.adg3736